論文 / 著書情報
Article / Book Information

題目(和文)	H[－]/O^{2－}混合アニオンを持つ層状ペロブスカイト遷移金属酸水素化物の合成と評価
Title(English)	Synthesis and Characterization of Layered Perovskite Transition-Metal Oxyhydrides with H[－]/O^{2－} Mixed Anion
著者(和文)	方俊皓
Author(English)	Joonho Bang
出典(和文)	学位:博士（工学）, 学位授与機関:東京工業大学, 報告番号:甲第9994号, 授与年月日:2015年9月25日, 学位の種別:課程博士, 審査員:細野　秀雄,神谷　利夫,平松　秀典,須崎　友文,阿藤　敏行,松石　聡
Citation(English)	Degree:Doctor (Engineering), Conferring organization: Tokyo Institute of Technology, Report number:甲第9994号, Conferred date:2015/9/25, Degree Type:Course doctor, Examiner:,,,,,
学位種別(和文)	博士論文
Type(English)	Doctoral Thesis

Synthesis and Characterization of Layered Perovskite Transition-Metal Oxyhydrides with H^-/O^{2-} Mixed Anion

Joonho Bang

Department of Materials Science and Engineering

Interdisciplinary Graduate School of Science and Engineering

Tokyo Institute of Technology

2015

Contents

Chapter 1 General Introduction

Oxygen is the third most abundant element in the universe and forms stable chemical bonds with almost all other elements, except for inert gases because of its electronegativity. For this reason, most of the Earth's crust consists of solid oxides and human civilization has been built by using these materials. As the understanding of materials science improves, the technology of humankind has reached the stage of application of metal oxides for electronic and magnetic purposes.

Recently, transition-metal (*TM*) oxides have attracted much attention because they have various intriguing physical properties. In *TM* oxides, the metal cations with partially filled *d* orbitals are regarded as interaction centers because most of the interesting electronic and magnetic interactions occur between them. Therefore, investigation of *TM* oxides has focused on the electronic structures of the metal cations and the interaction between them, whereas the anion has not received much attention because of its fully occupied *p* orbitals. However, it is important to focus on the role of intervening anions because they act as "bridging anions" that mediate *TM* cations.

The present study focuses on the role of hydride ions as a substitution element in *TM* oxides. In this chapter, the main concept, background, and objective of this study are summarized.

1.1 Background

1.1.1 Strongly correlated electron systems

According to band theory, materials can be classified as metals or insulators. For insulators, the highest filled band is completely filled, while for metals it is partially filled. Insulators with a small energy gap between the highest filled band and lowest empty band can be regarded as semiconductors because they become electrically conducting with thermal excitation of the electrons. However, for materials with partially filled *d* or *f* orbitals, the electrons experience strong Coulomb repulsion because of their spatial confinement in these orbitals. Therefore, it is difficult to explain their physical properties with conventional band theory. These materials have remarkably rich physical properties originating from the competing interactions between charge, spin, orbitals, and lattice degrees of freedom (**Figure 1-1**).

Layered perovskite-type *TM* oxides are a typical example of a strongly correlated electron system. These materials have various intriguing physical properties, such as high-temperature superconductivity,[1] colossal magnetoresistance,[2] Mott transitions,[1] and spin/orbital ordering.[3] The large variety of phenomena originate from various interactions, including on-site Coulomb, hopping, electron–phonon, and spin–orbit interactions, which mediate the coupling among the spin, orbital, charge, and lattice degrees of freedom.

Recently, the vanadium-based layered perovskite oxide Sr_2VO_4 has been investigated as a highly correlated electron system with strong orbital-ordering characters.[4–10] Sr_2VO_4 is a representative layered perovskite oxide, and has a tetragonal K_2NiF_4-type structure (space

group *I*4/*mmm*, **Figure 1-2**). The tetragonal elongation of the oxygen octahedra along the *c* axis partly lifts the threefold orbital degeneracy, i.e., the d_{xy} orbital is pushed to a higher energy, while the d_{xz} and d_{yz} orbitals remain degenerate. Recent reports have shown relatively strong spin–orbital coupling between the d_{xz} and d_{yz} orbitals (**Figure 1-3**),[8] even though vanadium is a 3*d TM*. Sr_2VO_4 is a Mott insulator (**Figure 1-4**) with a d^1 electronic configuration, and undergoes orbital ordering at around 100 K. A recent muon study reported the appearance of static antiferromagnetic (AFM) order below 8 K.[11]

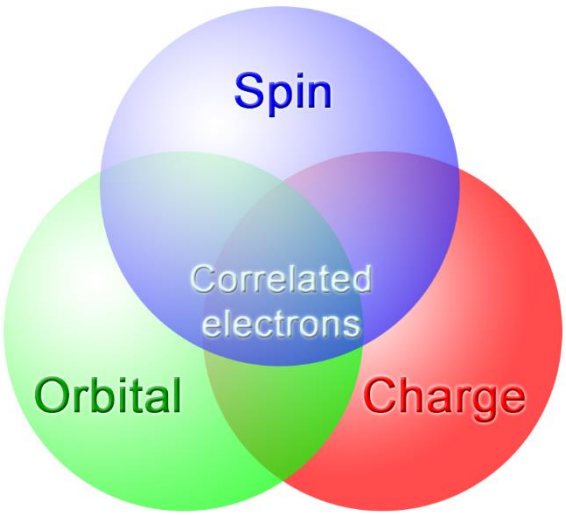

Figure 1-1. Schematic diagram showing the interplay between spin, orbital, and charge degrees of freedom in a strongly correlated electron system.

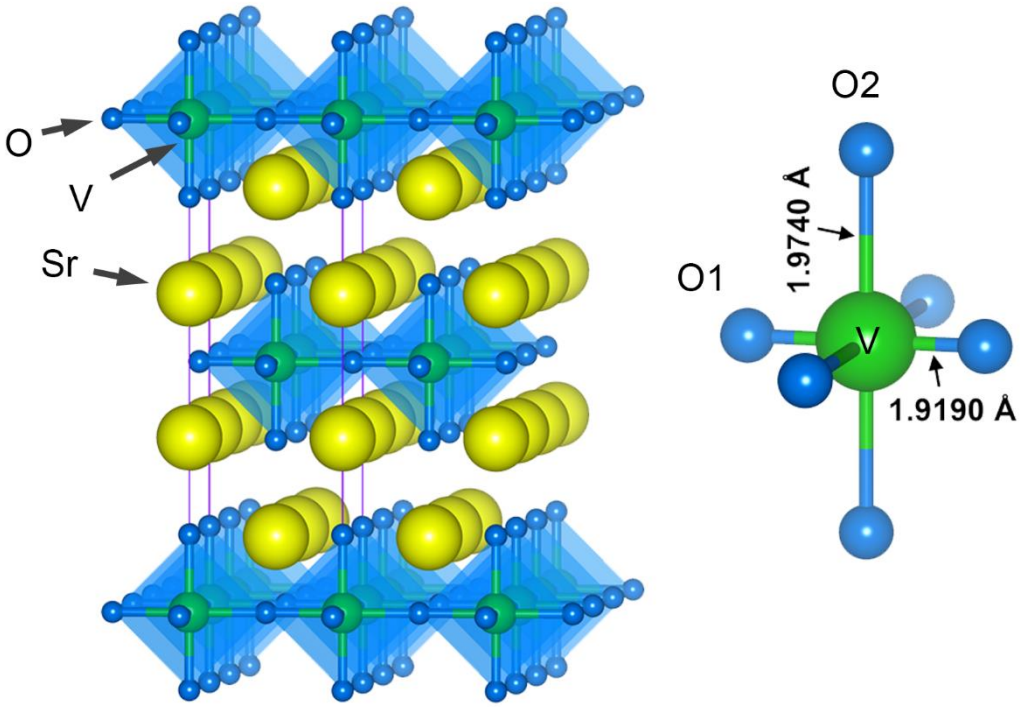

Figure 1-2. Crystal structure of Sr_2VO_4 and local geometry around the vanadium cation.

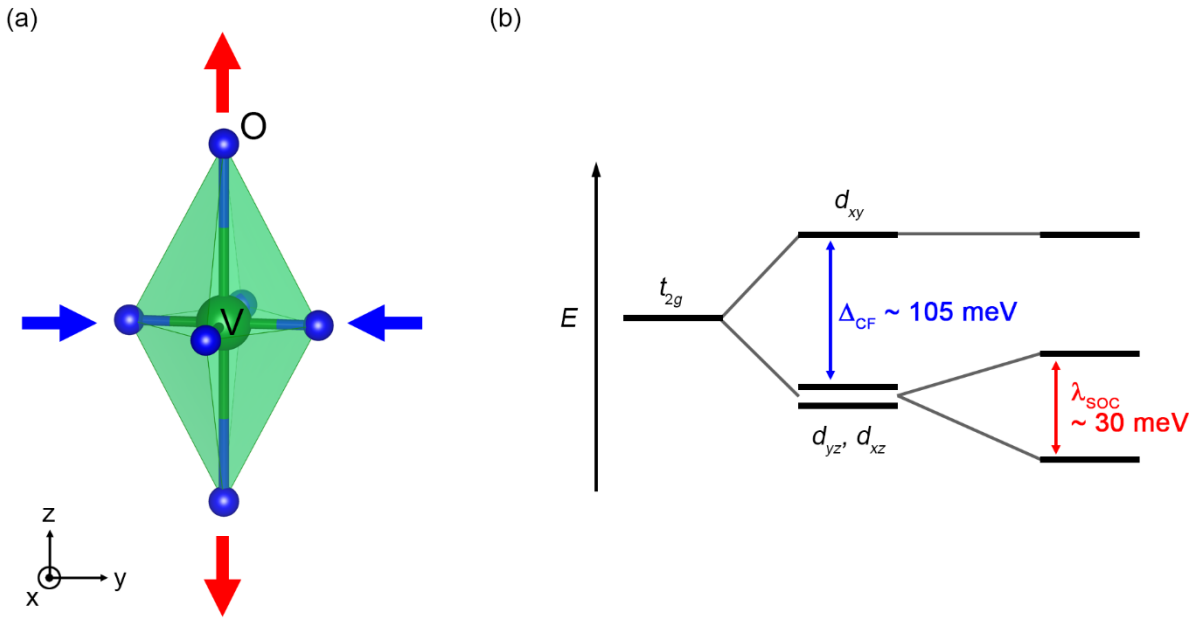

Figure 1-3. Energy level splitting of vanadium *d* orbitals by surrounding oxide ions. (a) Schematic diagram of the crystal field effect on the vanadium cation by surrounding oxide ions. (b) Energy level splitting of V t_{2g} bands by crystal field splitting (Δ_{CF}) and spin–orbit coupling (λ_{SOC}).

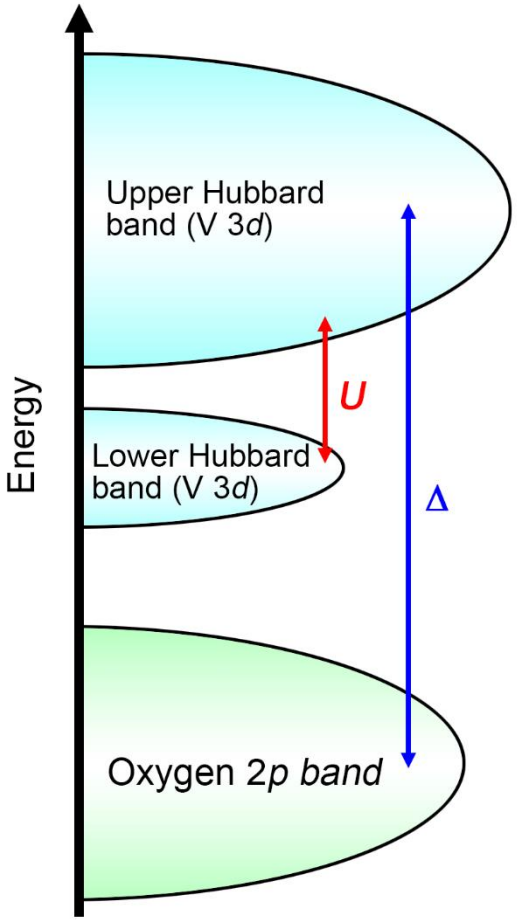

Figure 1-4. Schematic energy diagram of Mott–Hubbard type Sr_2VO_4.

1.1.2 Role of oxide ions in transition-metal oxides

The wide variety of interesting physical phenomena in *TM* oxides are usually caused by the electrons in the partially filled *d* orbitals of the metal cation, while the oxygen anion with fully occupied *p* orbitals does not directly participate in these interactions. However, the importance of the bridging oxygen anion connecting two metal cations by electrostatic attraction cannot be emphasized enough because it has a significant influence on the electronic structure of the metal *d* orbitals and the magnetic interactions between them. The importance of the bridging anion is more significant for strongly correlated electron systems because they are extremely sensitive to small changes in the chemical environment, such as orbital overlap.

The electronic structure of metal *d* orbitals is greatly affected by the surrounding anions.[12] For example, in the case of an octahedrally coordinated metal cation, the energies of the $d_{x^2-y^2}$ and d_{z^2} orbitals increase because of strong electrostatic repulsion with the *p* orbitals of ligand anions, while the energies of the d_{xy}, d_{yz}, and d_{xz} orbitals decrease with respect to this normal energy level (**Figure 1-5**). Because this ligand field splitting is strongly affected by both the geometric configuration and the orbital symmetry of surrounding anions, the role of the ligand anion is important to determine the physical properties of the materials.

Another important aspect of the anion is that it is the bridging medium for the magnetic interaction between metal cations.[13] For the superexchange interaction, it is important to consider the characteristics of the bridging anion because the superexchange interaction occurs through the intervening anion. The superexchange interaction can occur when the net overlap between the metal *d* orbital and the anion *p* orbital is not zero. However, when the orbitals between the metal cation and the bridging anion have an orthogonal relation (no net overlap),

the exchange interaction does not occur. **Figure 1-6** shows the possible orbital overlap between the metal cation and the bridging anion. The cation–anion–cation bond angle is also a crucial factor to determine the type of superexchange interaction. When the two cation orbitals overlap the same *p* orbital and are oriented at 180/90 °to the bridging anion, the interaction can be an AFM/ferromagnetic interaction.

The importance of the anion has led to the study of mixed-anion systems, such as oxyhalides, oxychalcogenides, and oxypnictides (**Figure 1-7**).[14–26] For these compounds, anion substitution is used as an electron/hole donor or to control the local structure, such as the interatomic distance and bonding angle. However, the interaction between the metal and the ligands is still restricted to "*d–p* bonding".

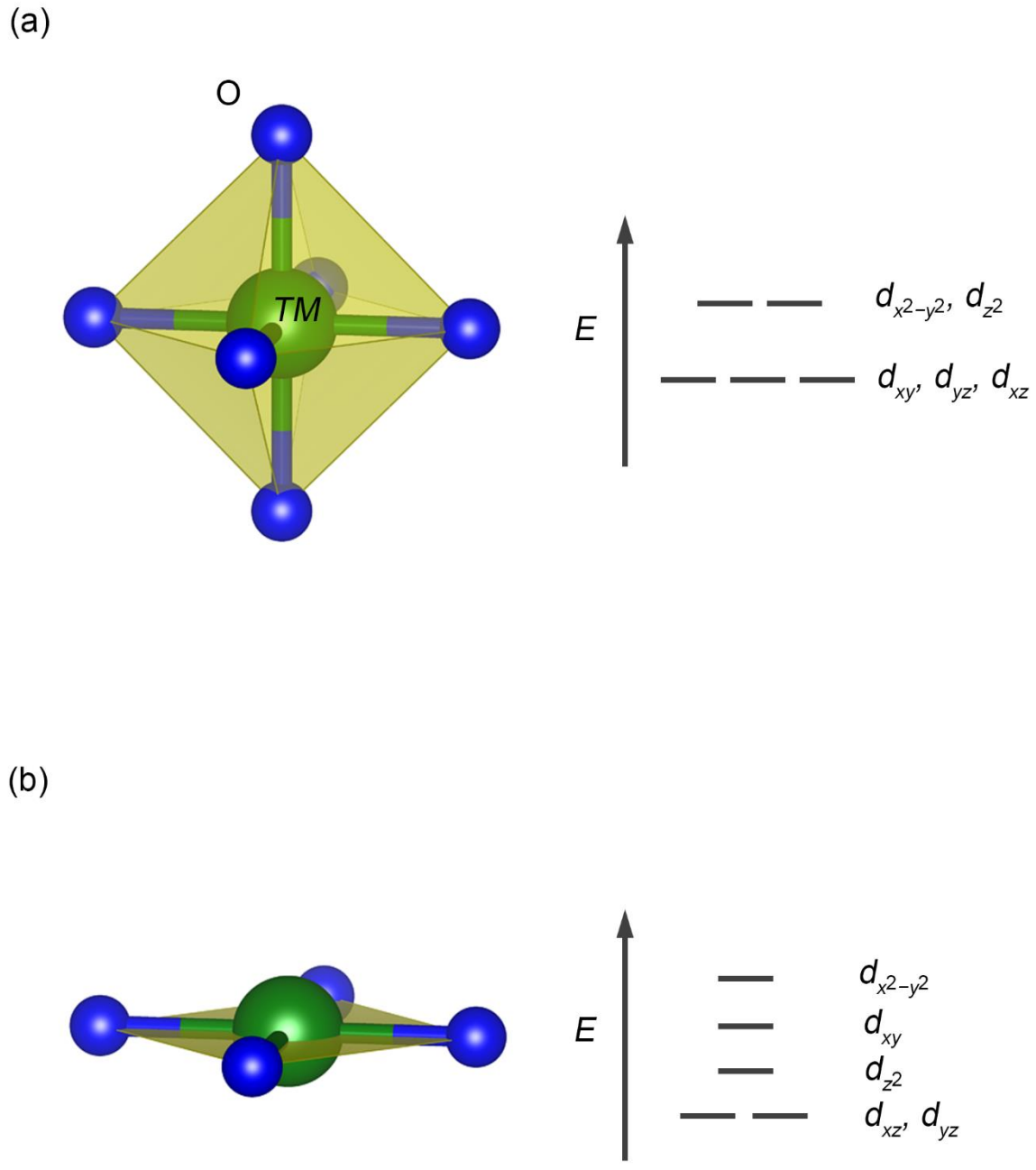

Figure 1-5. Energy level splitting of the *d* orbitals of the *TM* by the surrounding anions. (a) Octahedral coordination. (b) Square-planar coordination.

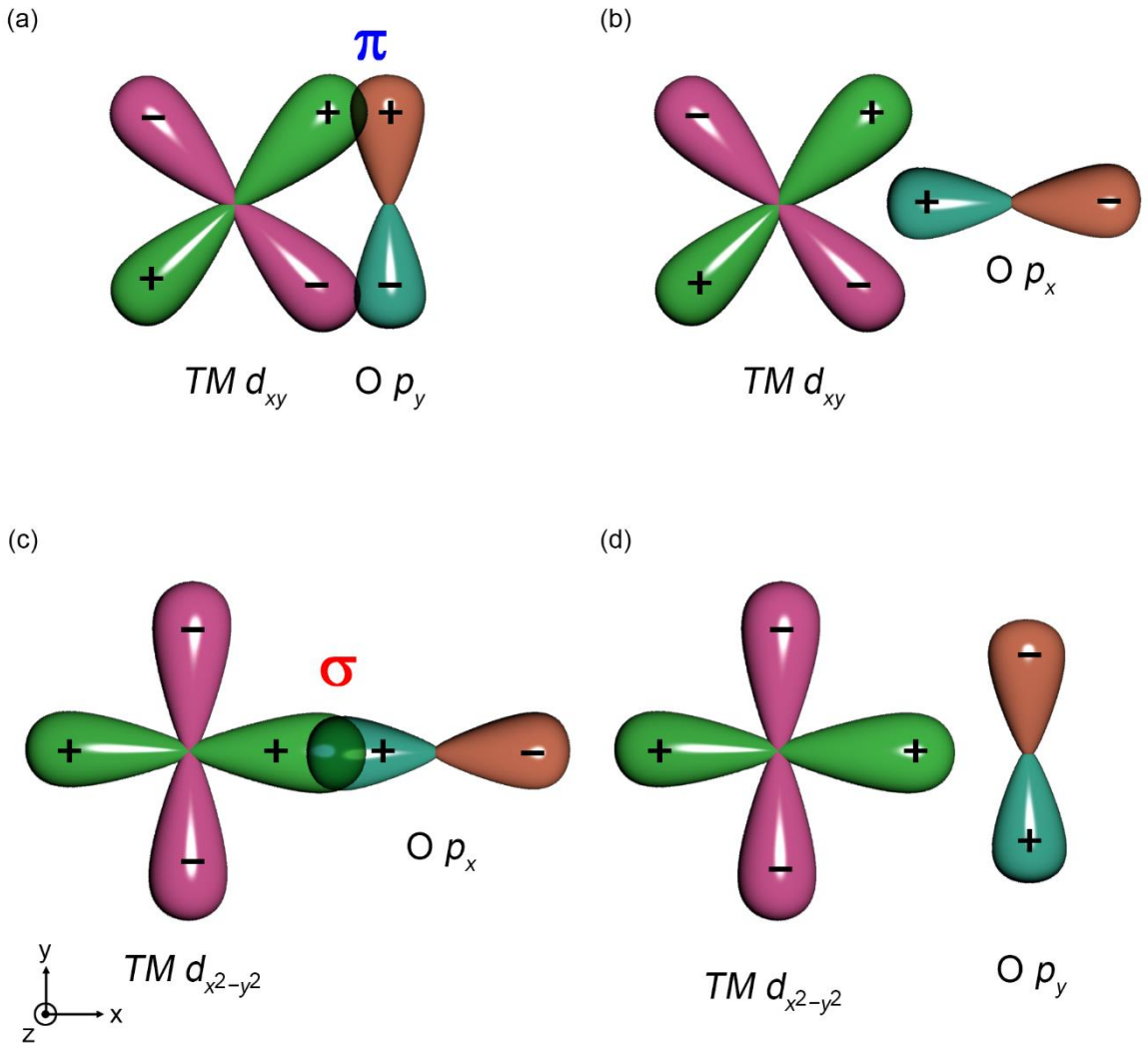

Figure 1-6. Symmetry relation of *TM* 3*d* and oxygen 2*p* orbitals. (a) π interaction (non-orthogonal). (b) Orthogonal. (c) σ interaction (non-orthogonal). (d) Orthogonal.

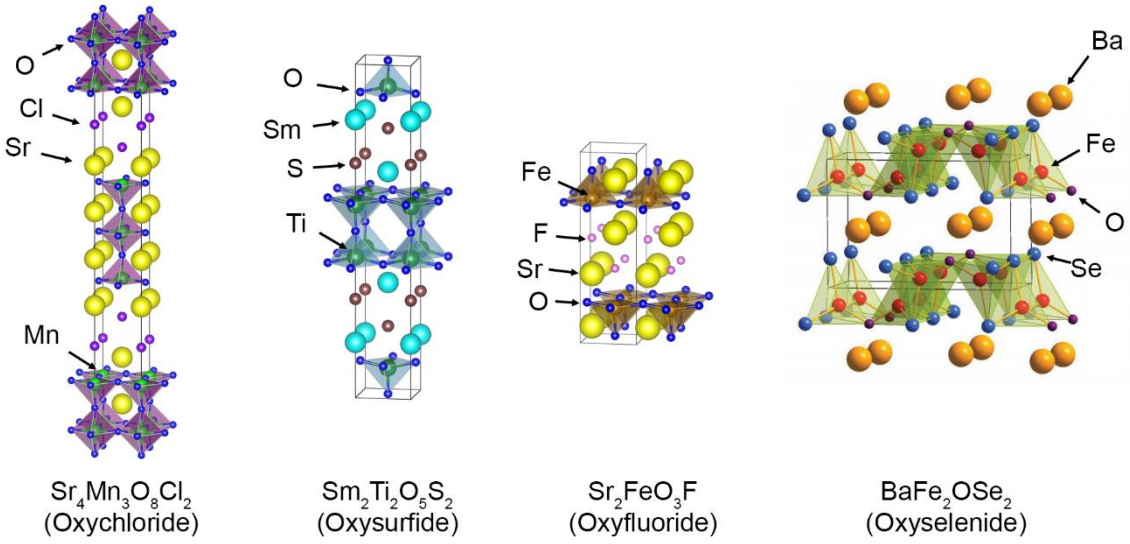

Figure 1-7. Various mixed-anion compounds containing oxygen ions.

1.1.3 Special characteristics of bipolar hydrogen

Hydrogen is the most abundant element in the universe and has a very rich chemistry despite its simple atomic structure (**Figure 1-8**). Although hydrogen is often placed in Group 1 in the periodic table because of its 1*s* valence orbital, this is not a true reflection of the chemical or physical properties of hydrogen.[27]

Hydrogen is the simplest bipolar element that can take three possible valence states (+1, 0, and −1). The proton (H^+) has a very high charge/radius ratio and is a very strong Lewis acid, so it easily bonds to other molecules and atoms, even He. In contrast, the hydride ion (H^-) shows strong reducing characteristics, so many metal hydrides, such as CaH_2 and SrH_2, are used as reducing agents in chemistry.[28,29]

The hydride ion is very high in the spectrochemical series because it is a strong σ donor.[27] Hydrogen can only form σ bonds in hydride compounds, and cannot form π bonds because of its spherical *s* orbital. In addition, the spatial spread of the H 1*s* orbital is sensitive to the chemical environment.[30] Because the ionic size is comparable with the oxide ion, so the hydride ion can be considered as a substitution element for the oxide ion, as an electron donor. From recent studies of iron-based superconductors, hydrogen substitution can achieve high concentration electron doping because of the stability of the hydride ion in rare-earth compounds (**Figure 1-9**).[31–33]

These unique characteristics of hydrogen are expected to provide a new pathway for mediating the electronic and magnetic interactions between *TM* cations. However, the synthesis of *TM* compounds including hydride ions is difficult because of the low decomposition

temperature of hydride compounds and the high reducing power of hydrogen.

From the viewpoint of structure analysis, the lack of core electrons to scatter X-rays means that bond distances and angles involving H atoms are difficult to measure by X-ray diffraction (XRD), so neutron diffraction is used when it is crucial to determine the precise positions and occupancies of H atoms (**Figure 1-10**).[34]

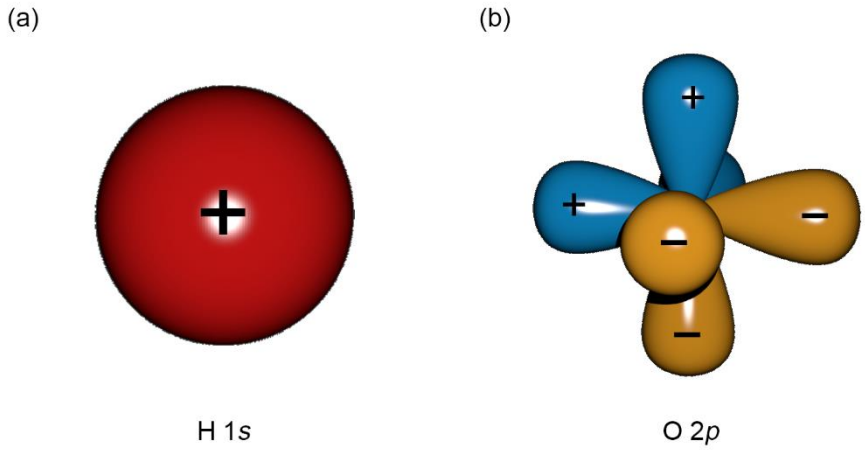

Figure 1-8. Comparison of the valence orbital symmetry of hydrogen and oxygen. (a) The spherical 1*s* orbital of hydrogen. (b) The three 2*p* orbitals (p_x, p_y, and p_z) of oxygen.

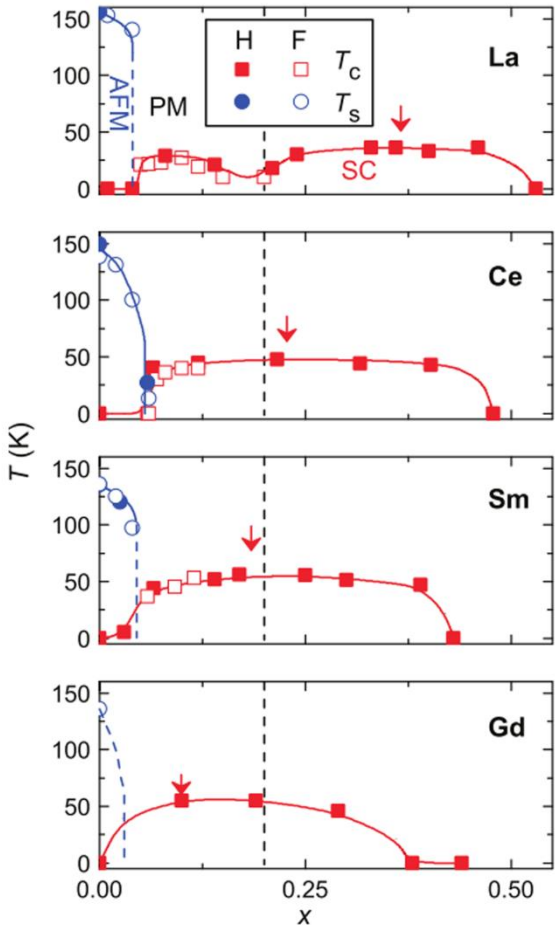

Figure 1-9. Superconducting phase diagrams of LnFeAsO$_{1-x}$H$_x$ (Ln = La, Ce, Sm, or Gd) and LnFeAsO$_{1-x}$F$_x$.[35] T_c is the critical temperature of superconductivity, and T_s is the anomalous kink in the temperature dependent resistivity curve.

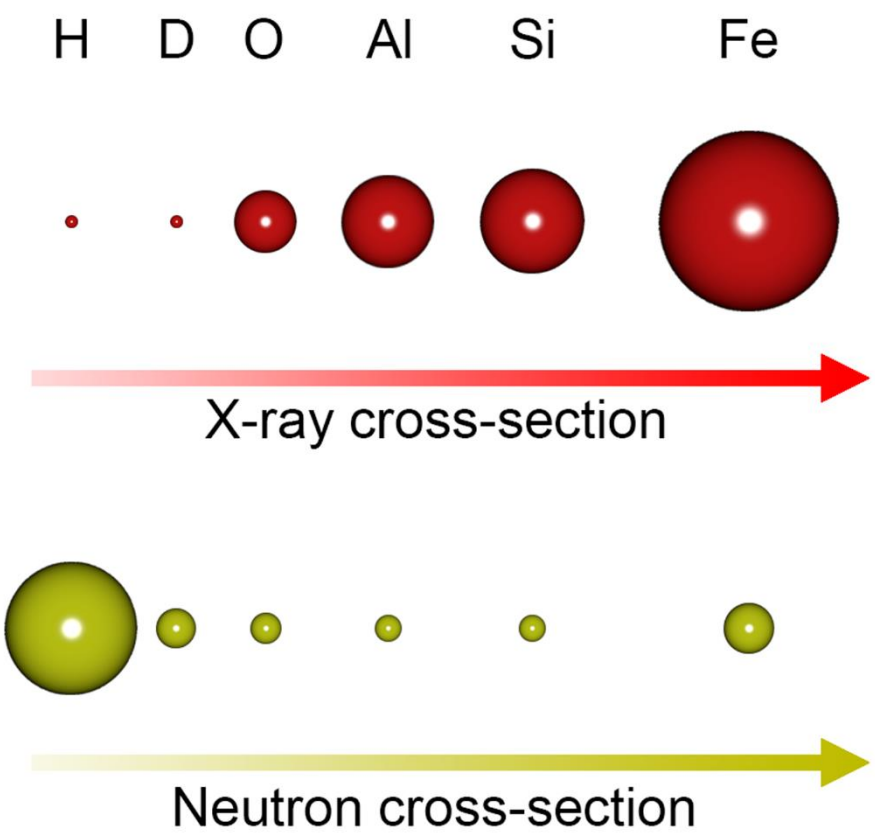

Figure 1-10. Comparison of the scattering cross-sections of X-ray and neutron diffraction.

1.1.4 High-pressure synthesis

The synthesis of materials under high pressure is a vast area of physics, chemistry, and engineering. This method is primarily associated with the successful synthesis of super-hard materials, such as diamond and cubic boron nitride. Recently, many new materials with novel physical properties have been successfully synthesized with the high-pressure method (**Figure 1-11**).[36–41]

When a material is subjected to high pressure, its crystal structure is usually compressed and this distortion is more effective for weak chemical bonds. Moreover, atomic bonds can become more covalent because of the decrease of the bond length, and phase transition to the closest-packed crystal structure can occur.[42] For synthesis of inorganic compounds, a pressure of several GPa can result in a meaningful volume change for metal or covalent/ionic substances with bulk moduli of ~100 GPa.[43]

There are several methods to realize high pressure with high temperature. Piston-cylinder- and Bridgman-anvil-type methods are the common methods for synthesis under high pressure. Piston-cylinder-type devices can press a relatively large volume (1–1000 cm^3), but the maximum pressure is not very high (~3 GPa). Much higher pressures can be produced in Bridgman-anvil-type devices, although the volume of the high-pressure zone is very small. To overcome these problems, the belt-type anvil device was invented (**Figure 1-12**). The high-pressure apparatus used in this study was a belt-type high-pressure anvil device, which can produce a pressure of more than 3 GPa for a larger volume than Bridgman-anvil-type devices.

Another application of high-pressure technology is introducing high hydrogen pressure. For example, abundant vacancies in Ni and Pd were successfully formed under high pressure

using hydrogen sources that desorb hydrogen under finite temperature.[44,45] Moreover, the hydrogen-incorporated iron-based superconductors $LnFeAsO_{1-x}H_x$ (*Ln* = La, Ce, Sm, or Gd) were successfully synthesized using high hydrogen pressure. This result indicates that the partial substitution of hydrogen in oxygen sites is possible using high-pressure synthesis.

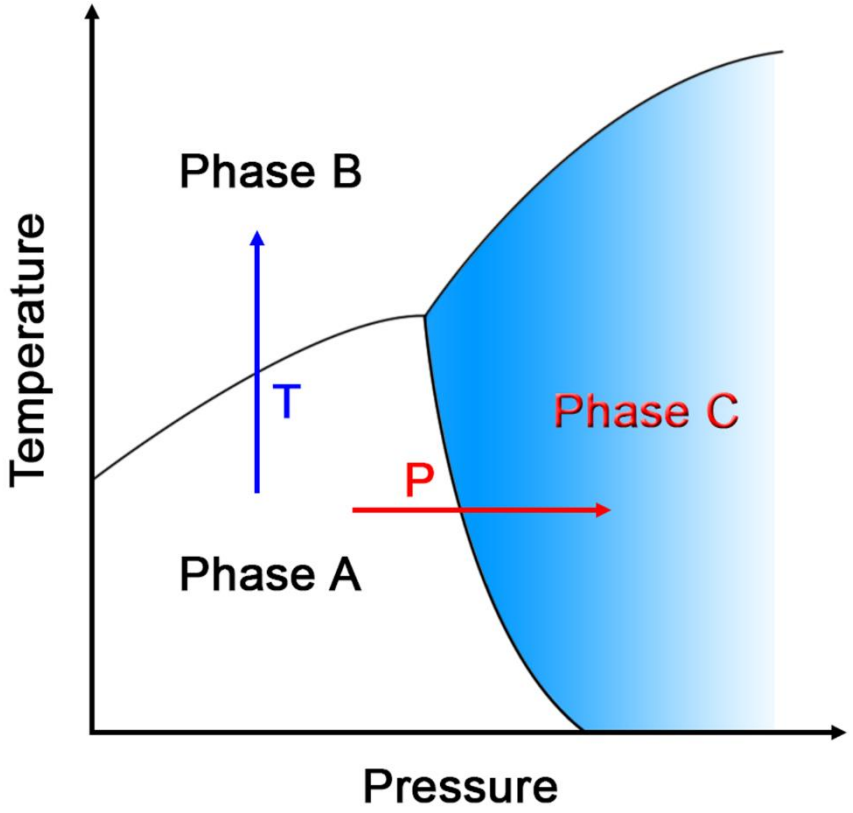

Figure 1-11. Schematic representation of a temperature and pressure dependent phase diagram. Note that phase C can only be obtained by high-pressure synthesis.

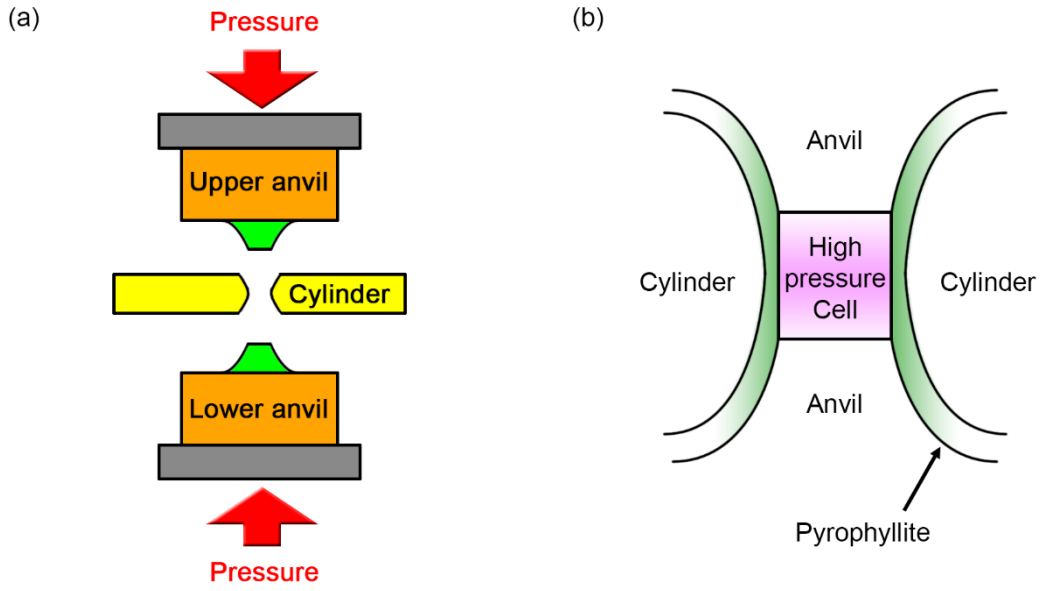

Figure 1-12. Schematic diagram of the belt-type anvil apparatus for high-pressure synthesis. (a) Pressure is applied by both the upper and lower anvils. (b) The high-pressure cell is surrounded by pyrophyllite, which is a solid pressure-transmitting medium.

1.2 Objective

Investigation of mixed-anion compounds is a promising way to discover families of functional *TM* compounds. Because the hydride ion has a spherically symmetrical 1*s* orbital, which is totally different from conventional ligand anions such as N^{3-}, O^{2-}, F^{-}, and Cl^{-}, this unique electronic nature provides the opportunity to realize compounds with novel physical and chemical properties. The present study was performed to clarify *the role of the hydride ion in the layered perovskite vanadium oxide system* by formation of "*d–s* bonding" through partial substitution of hydride ions in oxygen sites (**Figure 1-13**).

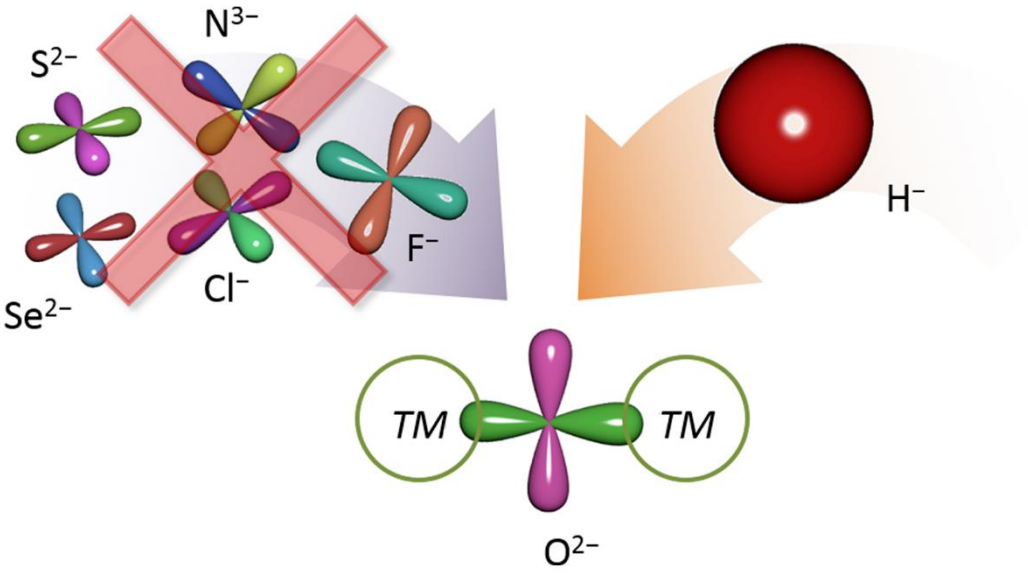

Figure 1-15. Schematic representation of the concept of this study.

1.3 Outline

Chapter 2 describes the synthesis of new layered perovskite vanadium oxyhydrides $Sr_2VO_{4-x}H_x$ ($0 < x < 1$) and their crystal structures. The hydrogen-ordering-induced structural phase transition is also discussed.

Chapter 3 describes low dimensionalization of magnetic ordering in a *TM* oxide Sr_2VO_4 by substitution of O^{2-} with H^-. The quasi-one-dimensional AFM spin-chain is induced in the three-dimensional crystal structure of Sr_2VO_3H.

Chapter 4 describes the origin of magnetic low dimensionalization in a *TM* oxyhydrides $Sr_2VO_{4-x}H_x$ by theoretical calculations. The anisotropic exchange interaction ($J_1/J_2 \sim 6$) in Sr_2VO_3H originated from the absence of π bonding between H 1*s* and V 3*d* orbitals.

Chapter 5 summarizes the results and gives the conclusions of the thesis.

References

1. M. Imada, A. Fujimori, and Y. Tokura, Rev. Mod. Phys. **70**, 1039 (1998).
2. *Colossal Magnetoresistive Oxides*, edited by Y. Tokura, Gordon and Breach, New York (2000).
3. Y. Tokura, Phys. Today **56**, 50 (2003).
4. M. Cyrot, B. Lambert-Andron, J. L. Soubeyroux, M. J. Rey, P. Dehauht, F. Cyrot-Lackmann, G. Fourcaudot, J. Beille, and J. L. Tholence, J. Solid State Chem. **85**, 321 (1990).
5. M. J. Rey, P. Dehaudt, J. C. Joubert, B. Lambert-Andron, M. Cyrot, and F. Cyrot-Lackmann, J. Solid State Chem. **86**, 101 (1990).
6. A. Nozaki, H. Yoshikawa, T. Wada, H. Yamauchi, and S. Tanaka, Phys. Rev. B **43**, 181 (1991).
7. H. D. Zhou, B. S. Conner, L. Balicas, and C. R. Wiebe, Phys. Rev. Lett. **99**, 136403 (2007).
8. H. D. Zhou, Y. J. Jo, J. Fiore Carpino, G. J. Munoz, C. R. Wiebe, J. G. Cheng, F. Rivadulla, and D. T. Adroja, Phys. Rev. B **81**, 212401 (2010).
9. M. V. Eremin, J. Deisenhofer, R. M. Eremina, J. Teyssier, D. van der Marel, and A. Loidl, Phys. Rev. B **84**, 212407 (2011).
10. J. Teyssier, R. Viennois, E. Giannini, R. M. Eremina, A. Günther, J. Deisenhofer, M. V. Eremin, and D. van der Marel, Phys. Rev. B **84**, 205130 (2011).

11. J. Sugiyama, H. Nozaki, I. Umegaki, W. Higemoto, E. J. Ansaldo, J. H. Brewer, H. Sakurai, T.-H. Kao, H.-D. Yang, and M. Månsson, Phys. Rev. B **89**, 020402 (2014).

12. *The Electronic Structure and Chemistry of Solids*, P. A. Cox (1987).

13. J. Kanamori, J. Phys. Chem. Solids **10**, 87 (1959).

14. M. AI-Mamouri, P. P. Edwards, C. Greaves, and M. Slaski, Nature **369**, 382 (1994).

15. S. M. Loureiro, C. Felser, Q. Huang, and R. J. Cava, Chem. Mater. **12**, 3181 (2000).

16. C.-Q. Jin, R. Puzniak, Z.-X. Zhao, X.-J. Wu, T. Tatsuski, T. Tamura, S. Adachi, K. Tanabe, H. Yamauchi, and S. Tanaka, Phys. Rev. B **61**, 778 (2000).

17. C. S. Knee and M. T. Weller, Chem. Commun. (Camb). **5**, 256 (2002).

18. S. J. Clarke, B. P. Guinot, C. W. Michie, M. J. C. Calmont, and M. J. Rosseinsky, Chem. Mater. **14**, 288 (2002).

19. C. S. Knee, M. A. L. Field, and M. T. Weller, Solid State Sci. **6**, 443 (2004).

20. M. Mortier, A. Bensalah, G. Dantelle, G. Patriarche, and D. Vivien, Opt. Mater. **29**, 1263 (2007).

21. R.-J. Xie and N. Hirosaki, Sci. Technol. Adv. Mater. **8**, 588 (2007).

22. S. J. Clarke, P. Adamson, S. J. C. Herkelrath, O. J. Rutt, D. R. Parker, M. J. Pitcher, and C. F. Smura, Inorg. Chem. **47**, 8473 (2008).

23. Y.-P. Du, Y.-W. Zhang, L.-D. Sun, and C.-H. Yan, J. Phys. Chem. C **112**, 405 (2008).

24. M. Yang, J. Oró-Solé, J. A. Rodgers, A. B. Jorge, A. Fuertes, and J. P. Attfield, Nat.

Chem. **3**, 47 (2011).

25. H. Lei, H. Ryu, V. Ivanovski, J. B. Warren, A. I. Frenkel, B. Cekic, W.-G. Yin, and C. Petrovic, Phys. Rev. B **86**, 195133 (2012).

26. E. J. Moon, Y. Xie, E. D. Laird, D. J. Keavney, C. Y. Li, and S. J. May, J. Am. Chem. Soc. **136**, 2224 (2014).

27. *Inorganic Chemistry, Fifth Edition*, P. W. Atkins, T. L. Overton, J. P. Rourke, M. T. Weller, (2010).

28. H. D. Kaesz and R. B. Saillant, Chem. Rev. **72**, 231 (1972).

29. W. Grochala and P. P. Edwards, Chem. Rev. **104**, 1283 (2004).

30. K. Hayashi, P. V. Sushko, Y. Hashimoto, A. L. Shluger, and H. Hosono, Nat. Commun. **5**, 3515 (2014).

31. T. Hanna, Y. Muraba, S. Matsuishi, N. Igawa, K. Kodama, S. Shamoto, and H. Hosono, Phys. Rev. B **84**, 024521 (2011).

32. S. Matsuishi, T. Hanna, Y. Muraba, S. W. Kim, J. E. Kim, M. Takata, S. Shamoto, R. I. Smith, and H. Hosono, Phys. Rev. B **85**, 014514 (2012).

33. S. Iimura, S. Matsuishi, H. Sato, T. Hanna, Y. Muraba, S. W. Kim, J. E. Kim, M. Takata, and H. Hosono, Nat. Commun. **3**, 943 (2012).

34. V. F. Sears, Neutron News **3**, 26 (2006).

35. H. Hosono and S. Matsuishi, Curr. Opin. Solid State Mater. Sci. **17**, 49 (2013).

36. J. A. Kafalas and J. M. Longo, J. Solid State Chem. **4**, 55 (1972).

37. E. Horvath-Bordon, R. Riedel, A. Zerr, P. F. McMillan, G. Auffermann, Y. Prots, W. Bronger, R. Kniep, and P. Kroll, Chem. Soc. Rev. **35**, 987 (2006).

38. Y. Inaguma, K. Hasumi, M. Yoshida, T. Ohba, and T. Katsumata, Inorg. Chem. **47**, 1868 (2008).

39. M. Yang, J. A. Rodgers, L. C. Middler, J. Or ó-Sol é, A. B. Jorge, A. Fuertes, and J. P. Attfield, Inorg. Chem. **48**, 11498 (2009).

40. Y. Shi, Y. Guo, Y. Shirako, W. Yi, X. Wang, A. A. Belik, Y. Matsushita, H. L. Feng, Y. Tsujimoto, M. Arai, N. Wang, M. Akaogi, and K. Yamaura, J. Am. Chem. Soc. **135**, 16507 (2013).

41. Y. Ding, C.-C. Chen, Q. Zeng, H.-S. Kim, M. J. Han, M. Balasubramanian, R. Gordon, F. Li, L. Bai, D. Popov, S. M. Heald, T. Gog, H. Mao, and M. van Veenendaal, Phys. Rev. Lett. **112**, 056401 (2014).

42. C. T. Prewitt and R. T. Downs, Rev. Mineral. **37**, 284 (1998).

43. V. V. Brazhkin, High Press. Res. **27**, 333 (2007).

44. Y. Fukai and N. Ōkuma, Jpn. J. Appl. Phys. **32**, L1256 (1993).

45. Y. Fukai and N. Ōkuma, Phys. Rev. Lett. **73**, 1640 (1994).

Chapter 2 Hydrogen Ordering and New Polymorph of Layered Perovskite Oxyhydrides: $Sr_2VO_{4-x}H_x$

2.1 Introduction

The design of functional materials is achieved based on a detailed understanding of the relationship between the material's properties and its atomic structure. In *TM* oxides, bonding interaction between *p* orbitals of oxygen anion and *d* orbitals of *TM* cation plays an important role in the physical properties of the materials.[1] At this point, exploration of mixed-anion compounds such as oxyhydrides is a promising way of discovering families of functional *TM* compounds.[2] The bipolar element hydrogen can have valence states from −1 to +1. In addition, the spatial spread of the H 1*s* orbital is sensitive to the chemical environment.[3] These unique characteristics of hydrogen are expected to provide a new pathway for mediating electronic and magnetic interactions.[2,4] Although several *TM* oxyhydride compounds have been reported to date, the well-controlled synthesis of these compounds is rather difficult because of opposite chemical nature of hydrogen and oxygen.[2,5–7] Two roles are expected for partial replacement oxygen sites by hydrogen in oxides. One is to serve as an effective electron donor. A clear-cut example utilizing this role was recently reported in iron-base superconductors $LaFeAsO_{1-x}H_x$ (where $0 \leq x \leq 0.5$).[8,9] The other is to work as a unique ligand to a *TM* cation because an orbital available for H^- is limited to 1s, which rather differs from the case of O^{2-}.

Sr_2VO_4 is a representative layered perovskite oxide and has a tetragonal K_2NiF_4-type structure (space group: *I*4/*mmm*)[10,11] composed of two-dimensional networks of corner-shared nondistorted VO_6 octahedra. This framework is the intergrowth of rock-salt *A*O block and perovskite *AB*O_3 unit, and the structures are well known to exhibit various intriguing physical phenomena such as high T_c superconductor $La_{2-x}Sr_xCuO_4$. This compound is a Mott insulator with a d^1 electronic configuration, and has an orbital-ordering transition around 100 K.[12] This chapter reports an investigation of the crystal structures and solid-state properties of $Sr_2VO_{4-x}H_x$ ($0.0 \leq x \leq 1.01$) with controlling of the hydrogen/oxygen amounts in a coordination sphere of vanadium metal cation. Oxygen/hydrogen ordering was observed by substitution, and a new orthorhombic polymorph was uncovered in highly hydrogen-substituted regions. Incorporation of controllable amount of hydrogen anion to the oxygen site without considerable oxygen-vacancy makes it possible to tune the valence state of vanadium cation from d^1 (V^{4+}) to d^2 (V^{3+}) by electron doping. Moreover, the structural stabilization can be expected by switching the HOMO level from the ($d\pi$–$p\pi$)* antibonding molecular orbital to a lower energy $d\sigma$–$s\sigma$ bonding orbital because hydrogen anion has no other orbital except 1*s*.

2.2 Experimental details

The oxyhydrides $LaSrCoO_3H_{0.7}$ and $ATiO_{3-x}H_x$ (A = Ca, Sr, and Ba) were synthesized by a topochemical reaction using reducing agents of NaH or CaH_2.[2,7] In the present study, the advanced high hydrogen pressure method is applied to synthesize oxyhydrides, which enables control of the hydrogen content and surpasses the substitution limit of the topochemical method.[13,14] Polycrystalline samples of $Sr_2VO_{4-x}H_x$ in the form of sintered pellets were synthesized by solid-state reaction using a belt-type high-pressure anvil cell, $(2-x)SrO + VO_2 + xSrH_2 \rightarrow Sr_2VO_{4-x}H_x + 0.5xH_2$. SrH_2 was prepared by heating strontium metal in a hydrogen atmosphere. All precursors were mixed in a glovebox filled with purified argon gas (H_2O, O_2 < 1 ppm). The starting mixture was placed in a BN capsule and sandwiched between pellets of external hydrogen source. The external hydrogen source was a mixture of $NaBH_4 + Ca(OH)_2$, which releases hydrogen gas during synthesis (**Figure 2-1**). The solid-state reaction was performed at 1473 K and 5 GPa for 30 min. BN separators blocked the passage of all reaction products except hydrogen gas. Both the sample and the hydrogen source were enclosed in a NaCl capsule (a hydrogen sealant) that was surrounded by a graphite tube heater and pyrophyllite as a solid pressure-transmitting medium.

Each sample was characterized by powder XRD using a Bruker D8 Advance diffractometer with Cu K_α radiation. Neutron powder diffraction (NPD) was performed using a neutron total scattering spectrometer (NOVA) installed in the Japan Proton Accelerator Research Complex (J-PARC). The powder diffraction data were measured at room temperature for ~8 h in a vanadium–nickel alloy holder with a diameter of 6 mm. Synchrotron powder XRD measurements were performed using the curved imaging plate diffractometer (BL-8A) at the

Photon Factory in High Energy Accelerator Research Organization (KEK-PF). The data were analyzed by the Rietveld method using TOPAS,[15] GSAS,[16,17] and RIETAN-FP.[18] The hydrogen concentrations in the samples were analyzed by thermal desorption spectroscopy (TDS) measurements (TDS1200, ESCO). The TDS measurements were carried out in a vacuum chamber with a background pressure of ~10^{-7} Pa at various temperatures from room temperature to 1273 K at a heating rate of 60 K/min. To examine the structural stability, density functional theory (DFT) calculations were performed using the generalized gradient approximation with the Perdew–Burke–Ernzerhof functional[19,20] and the projected augmented plane-wave method[21] implemented in the Vienna ab initio simulation program code (VASP).[22] A $2a \times 2a \times c$ supercell containing nine chemical formulas was used, and the plane-wave basis set cutoff was set to 800 eV. The lattice parameters of each cell were specified using linear fitting of lattice parameters collected by Rietveld fitting of the NPD data. To calculate the total energy, $9 \times 9 \times 6$ *k*-point grids were used.

2.3 Results and Discussion

Because the synthesized $Sr_2VO_{4-x}H_x$ samples were stable in an ambient atmosphere, their characterization was performed in ambient conditions. **Figure 2-2** shows the XRD patterns and the lattice parameters *a*, *b*, and *c* of $Sr_2VO_{4-x}H_x$ collected by XRD patterns with different nominal *x* values (x_{nom}) in the starting mixture. For $x_{nom} \leq 0.7$, the XRD patterns were indexed by the *I*4/*mmm* tetragonal phase. It was found that there were linear relationships between the lattice parameters and x_{nom}. Sr_2VO_4 crystallizes in a tetragonal phase with a *c*/*a* ratio of 3.27, which increases to 3.34 (+2.14%) for $x_{nom} = 0.7$. At $x_{nom} = 0.8$, a tetragonal (*I*4/*mmm*)-to-orthorhombic (*Immm*) phase change was observed with a large difference between *a* and *b* ($b - a = 0.2037$ Å at $x_{nom} = 1.2$). For $x_{nom} > 1.2$, variation in lattice constants was saturated.

NPD, which is suited for the investigation of the oxygen and hydrogen sites in crystals, was performed to determine the detailed crystal structures. The NPD patterns for $x_{nom} = 0.0$, 0.5, and 1.2 are shown in **Figure 2-3**. The crystal of Sr_2VO_4 ($x_{nom} = 0.0$) has vacancies in 2% of the oxygen sites, which were randomly located at both the equatorial (O1) and apical (O2) oxygen positions in the VO_2 layers. The crystal structures and local geometries of the $Sr_2VO_{4-x}H_x$ derived from the NPD data are shown in **Figure 2-4** and its lattice parameters are summarized in **Table 2-1**. When $x_{nom} = 0.5$ of hydrogen was introduced into the crystal lattice, the V–O1 length decreased by 0.52%, but the V–O2 length increased by 1.11% with increase of the *c*/*a* ratio. The bond length ratios between V–O1 and V–O2, *d*(V–O2)/*d*(V–O1), were 1.030 and 1.047 for $x_{nom} = 0.0$ and 0.5, respectively.

Figure 2-5 shows the TDS data of the $Sr_2VO_{4-x}H_x$ samples with various hydrogen contents. As x_{nom} was increased from 0.3 to 1.4, the amount of hydrogen released as H_2

gradually increased from 0.25 to 1.24 per formula unit. It was also found that there was broadening of the desorption range and an increase in the number of desorption peaks, which is probably related to the local environment of each hydrogen anion. Considering that the occupation of hydrogen in the O1 site, which has a shorter bond length with V than hydrogen in the O2 site, gradually increased with increasing x_{meas}, it appears to be reasonable that the upper limit of the desorption temperature gradually increased in the TDS data. **Figure 2-6** shows the amounts of hydrogen and oxygen vacancies in the samples as a function of x_{nom}. The amount of hydrogen was obtained by integrating the thermal desorption spectrum, and the amount of oxygen vacancies was estimated by refining the synchrotron x-ray data (**Figure 2-7**). It was found that the amount of hydrogen in the sample (x_{meas}) linearly increased with increasing x_{nom}.

For x_{nom} = 0.5 and 1.2, Rietveld refinement of NPD data was performed under constraints consistent with the hydrogen contents obtained by TDS. As a result, the compositions of $Sr_2VO_{3.62}H_{0.38}$ and $Sr_2VO_{2.99}H_{1.01}$ were obtained for x_{nom} = 0.5 and 1.2, respectively. It was found that the residual factor of refinement R_{wp} value decreased monotonically with a decrease in anion site vacancy when R_{wp} was examined as a function of vacancy fraction for each anion site (**Figure 2-8** and **Figure 2-9**). This finding means that the vacancy-free model was appropriate for $Sr_2VO_{4-x}H_x$, and this result is in contrast with known layered oxyhydrides such as $LaSrCoO_3H_{0.7}$ and $Sr_3Co_2O_{4.33}H_{0.84}$, where anion vacancies play an important role in stabilizing the crystal structure.[5] The present experimental finding appears to be related to the different synthetic route, i.e., under high-pressure synthetic conditions, oxygen vacancies can be easily filled by H^- owing to combined effects of the high hydrogen pressure in the closed

system and stronger covalent nature between V-H which results in the stabilization of hydrogen anion than oxygen vacancy.

It was also found that hydrogen in $Sr_2VO_{3.62}H_{0.38}$ shows site selectivity even though the structural phase transition had not yet occurred. In mixed anion compounds with layered structures, there was a strong tendency for isolation of different anions in each site. Therefore, sharing of structurally indistinct sites in the same plane by hydrogen and oxygen is difficult.[5] However, for $Sr_2VO_{3.62}H_{0.38}$, 79% of the hydrogen anions were located at the O1 site, and the O2 site was occupied by 21% of hydrogen anions coexisting with oxygen anions, i.e., a mixed-anion state. For $Sr_2VO_{2.99}H_{1.01}$, 97% of the hydrogen anions were located in the V–O plane, and stripe-type ordering of oxygen (O1) and hydrogen (H1) occurred along with the appearance of a new phase by shortening of the V–H1 bond length. Our high-pressure synthesis method with an excess of hydrogen realizes a wide range of hydrogen substitution into oxygen sites without considerable oxygen vacancy.

Figure 2-10a shows the degree of anion ordering as a function of x_{meas}. In the low hydrogen substitution region ($x_{meas} < 0.25$), hydrogen anions statistically occupy both O1 and O2 sites. With higher hydrogen substitution ($x_{meas} > 0.25$), hydrogen anions tend to occupy the oxygen sites in the V–O planes (i.e., the O1 site). Finally, most of hydrogen anions occupy sites in the V–O planes, and a crystallographic phase transition occurs. **Figure 2-10b** shows the calculated total energy difference (ΔE) between E_1 for H in the O1 site and E_2 for H in the O2 site. In the first stage of x, ΔE is so small that anion ordering does not increase the structural stability. When $x > 0.25$, ΔE starts to decrease, indicating that the system becomes relatively

more stable when hydrogen is located in the O1 site. When $x \sim 0.25$, a disorder-to-order transition of hydrogen occurs, which is consistent with calculations of the total energy.

A major difference between H^- and O^{2-} is their electronic structures. Hydrogen has only a 1*s* orbital available for chemical bonding, whereas the oxygen anion has three available 2*p* orbitals. As shown in **Figure 2-11**, O^{2-} behaves as a π-donor ligand and its *p* orbitals have net overlap with the V d_{xy}, d_{xz}, and d_{yz} orbitals, forming bonding (π) and antibonding (π^*) molecular orbitals. The electrons supplied by the oxygen occupy the $d\pi$–$p\pi$ bonding orbitals, whereas an electron originally belonging to the triply degenerate V 3*d* orbitals (d_{xy}, d_{xz}, and d_{yz}) occupies the antibonding orbital. In contrast, the hydrogen anion has no orbitals that have the same symmetry as the V d_{xy}, d_{xz}, and d_{yz} orbitals, so the V d_{xy}, d_{xz}, and d_{yz} orbitals remain nonbonding and are fully localized on the vanadium cation. However, the H^- anion can form strong σ bonds with doubly degenerate V 3*d* orbitals (d_{x2-y2}, d_{z2}). Therefore, when O^{2-} is substituted by H^-, the occupancy in the antibonding orbital decreases, and consequently the total energy of the crystal decreases. The extent of this stabilization should depend on the local environment of hydrogen. In the case of the O1 site, oxygen is coordinated to six cations, 4Sr + 2V, while in the O2 site oxygen is coordinated to 5Sr + 1V. Therefore, when hydrogen is introduced into the O1 site, the stabilization effect is much greater than when it is introduced in the O2 site. The hydrogen substitution-induced phase transition results in the sudden change of the bonding interactions. Because the V–O1 bond length gradually decreases with increasing *x*, the antibonding interaction between V and O1 increases. This structural instability causes elongation of the V–O bonds by the structural transition.

2.4 Conclusion

In this chapter, new vanadium-based layered perovskite oxyhydrides $Sr_2VO_{4-x}H_x$ were synthesized, and the hydrogen and oxygen concentrations were successfully controlled in the full range ($0.0 \leq x \leq 1.01$) without any considerable anion-vacancies. This result makes it possible for application of a hydride ion as an effective carrier dopant in oxides and open up the new method for tuning exchange interaction between the *TM* cations. Moreover, by controlling the hydrogen amount, mixed anion region was uncovered, and it was found that the hydrogen ordering induced structural transition and structural stabilizing effect of hydrogen anion substitution. The theoretical calculations suggest that the degree of oxygen/hydrogen anion ordering is strongly correlated with reduction of antibonding interactions between vanadium and the oxygen ligands.

References

1. M. Imada, A. Fujimori, and Y. Tokura, Rev. Mod. Phys. **70**, 1039 (1998).
2. M. A. Hayward, E. J. Cussen, J. B. Claridge, M. Bieringer, M. J. Rosseinsky, C. J. Kiely, S. J. Blundell, I. M. Marshall, and F. L. Pratt, Science **295**, 1882 (2002).
3. K. Hayashi, P. V. Sushko, Y. Hashimoto, A. L. Shluger, and H. Hosono, Nat. Commun. **5**, (2014).
4. K. Poeppelmeier, Science **295**, 1849 (2002).
5. R. M. Helps, N. H. Rees, and M. A. Hayward, Inorg. Chem. **49**, 11062 (2010).
6. T. Sakaguchi, Y. Kobayashi, T. Yajima, M. Ohkura, C. Tassel, F. Takeiri, S. Mitsuoka, H. Ohkubo, T. Yamamoto, J. Kim, N. Tsuji, A. Fujihara, Y. Matsushita, J. Hester, M. Avdeev, K. Ohoyama, and H. Kageyama, Inorg. Chem. **51**, 11371 (2012).
7. Y. Kobayashi, O. J. Hernandez, T. Sakaguchi, T. Yajima, T. Roisnel, Y. Tsujimoto, M. Morita, Y. Noda, Y. Mogami, A. Kitada, M. Ohkura, S. Hosokawa, Z. Li, K. Hayashi, Y. Kusano, J. Kim, N. Tsuji, A. Fujiwara, Y. Matsushita, K. Yoshimura, K. Takegoshi, M. Inoue, M. Takano, and H. Kageyama, Nat. Mater. **11**, 507 (2012).
8. M. Hiraishi, S. Iimura, K. M. Kojima, J. Yamaura, H. Hiraka, K. Ikeda, P. Miao, Y. Ishikawa, S. Torii, M. Miyazaki, I. Yamauchi, A. Koda, K. Ishii, M. Yoshida, J. Mizuki, R. Kadono, R. Kumai, T. Kamiyama, T. Otomo, Y. Murakami, S. Matsuishi, and H. Hosono, Nat. Phys. **10**, 300 (2014).
9. S. Iimura, S. Matsuishi, H. Sato, T. Hanna, Y. Muraba, S. W. Kim, J. E. Kim, M. Takata,

and H. Hosono, Nat. Commun. **3**, 943 (2012).

10. M. Cyrot, B. Lambert-Andron, J. L. Soubeyroux, M. J. Rey, P. Dehauht, F. Cyrot-Lackmann, G. Fourcaudot, J. Beille, and J. L. Tholence, J. Solid State Chem. **85**, 321 (1990).
11. M. J. Rey, P. Dehaudt, J. C. Joubert, B. Lambert-Andron, M. Cyrot, and F. Cyrot-Lackmann, J. Solid State Chem. **86**, 101 (1990).
12. H. D. Zhou, B. S. Conner, L. Balicas, and C. R. Wiebe, Phys. Rev. Lett. **99**, 136403 (2007).
13. Y. Fukai and N. Ōkuma, Phys. Rev. Lett. **73**, 1640 (1994).
14. Y. Fukai and N. Ōkuma, Jpn. J. Appl. Phys. **32**, L1256 (1993).
15. TOPAS; Bruker AXS GmbH: Karlsruhe, Germany, 2009.
16. Larson A.C. and Von Dreele R.B., Los Alamos Natl. Lab. Rep. LAUR 86 (2000).
17. B. H. Toby, J. Appl. Crystallogr. **34**, 210 (2001).
18. F. Izumi and K. Momma, Solid State Phenom. **130**, 15 (2007).
19. J. P. Perdew, K. Burke, and M. Ernzerhof, Phys. Rev. Lett. **77**, 3865 (1996).
20. J. P. Perdew, K. Burke, and M. Ernzerhof, Phys. Rev. Lett. **78**, 1396 (1997).
21. P. E. Blöchl, Phys. Rev. B **50**, 17953 (1994).
22. G. Kresse, Phys. Rev. B **54**, 11169 (1996).

Figures

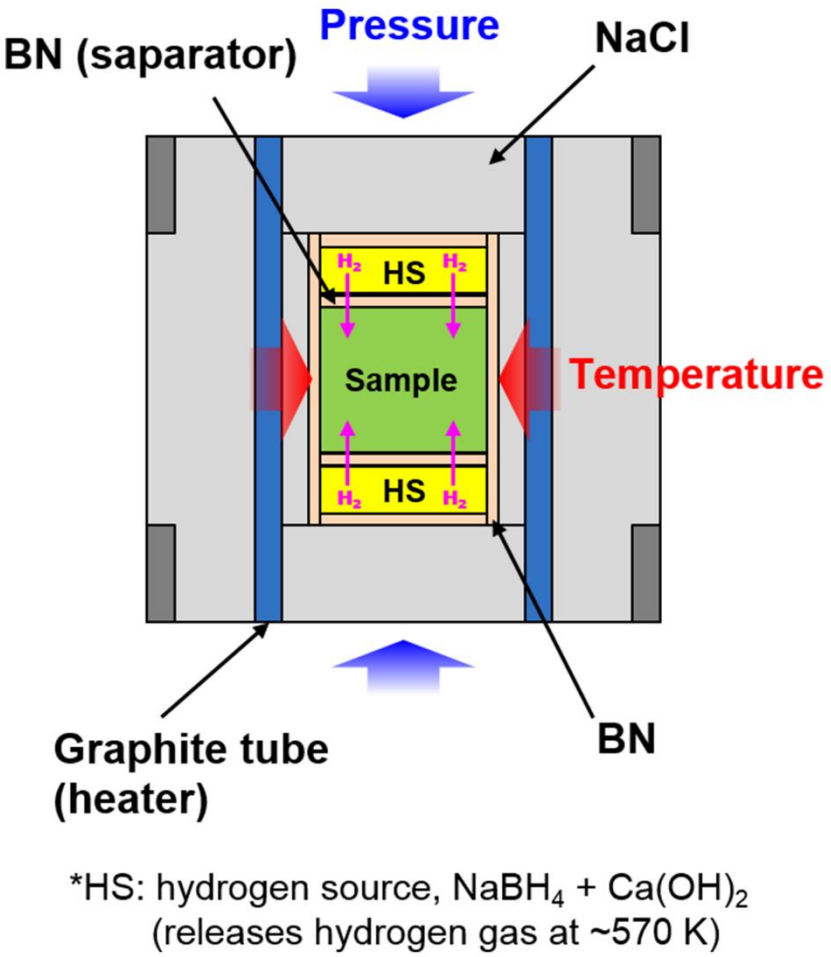

Figure 2-1. Schematics of a high pressure cell for belt-type high pressure apparatus.

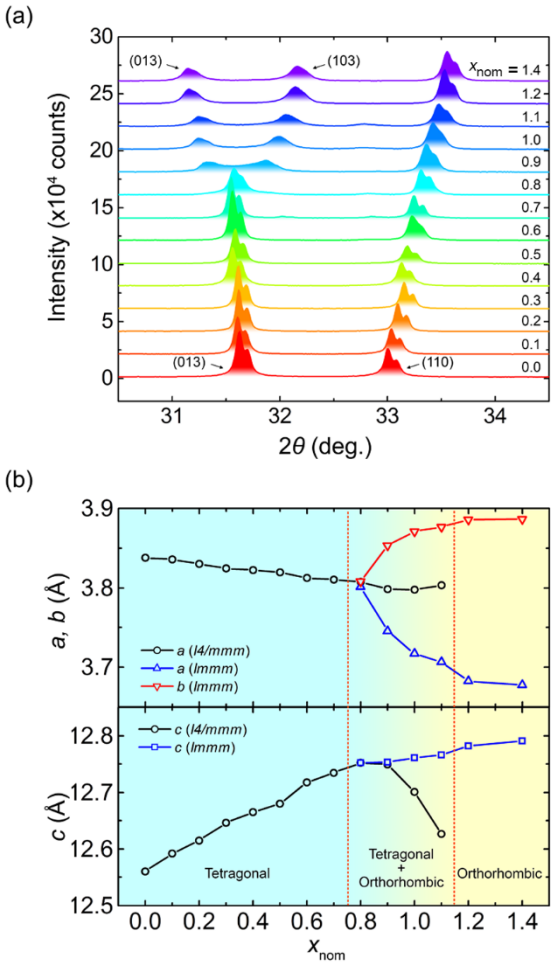

Figure 2-2. Structural data from the XRD measurements of $Sr_2VO_{4-x}H_x$. (a) Powder XRD patterns of $Sr_2VO_{4-x}H_x$. (b) Lattice parameters from the XRD data as a function of x_{nom}.

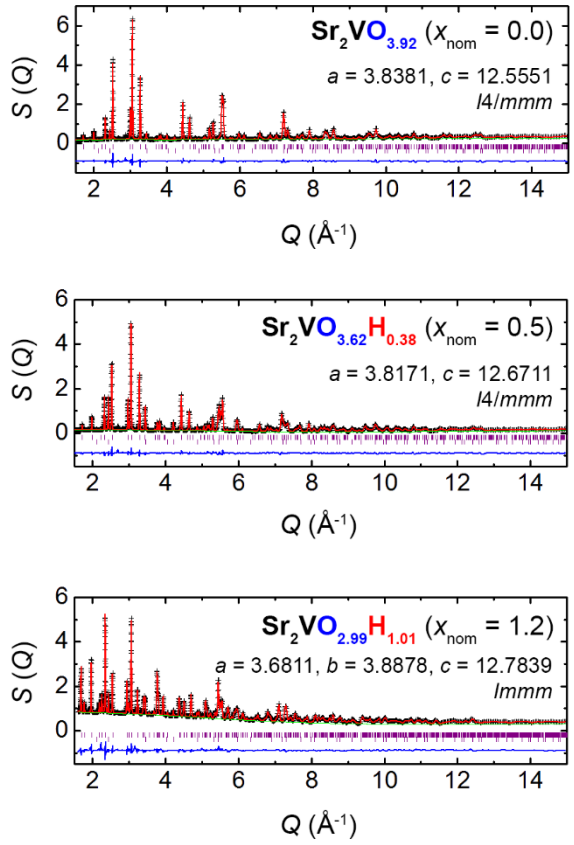

Figure 2-3. NPD patterns with Rietveld fitting of $Sr_2VO_{4-x}H_x$ (x_{nom} = 0.0, 0.5, and 1.2). The data were collected using NOVA (90 °bank) at 300 K.

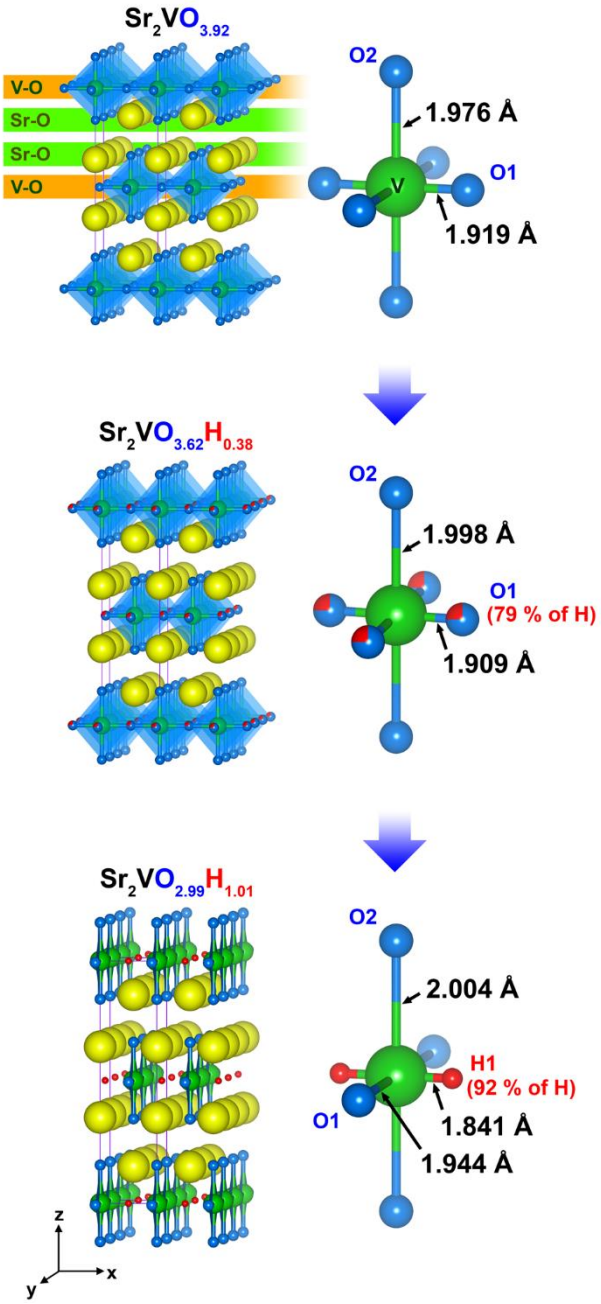

Figure 2-4. Crystal structure of $Sr_2VO_{4-x}H_x$ (x_{nom} = 0.0, 0.5, and 1.2) and local geometry around vanadium cation. Structure analyses from NPD data indicate compositions of $Sr_2VO_{3.62}H_{0.38}$ and $Sr_2VO_{2.99}H_{1.01}$ for x_{nom} = 0.5 and 1.2, respectively. 79% ($Sr_2VO_{3.62}H_{0.38}$) and 97% ($Sr_2VO_{2.99}H_{1.01}$) of hydrogen anions are ordered in V–O planes.

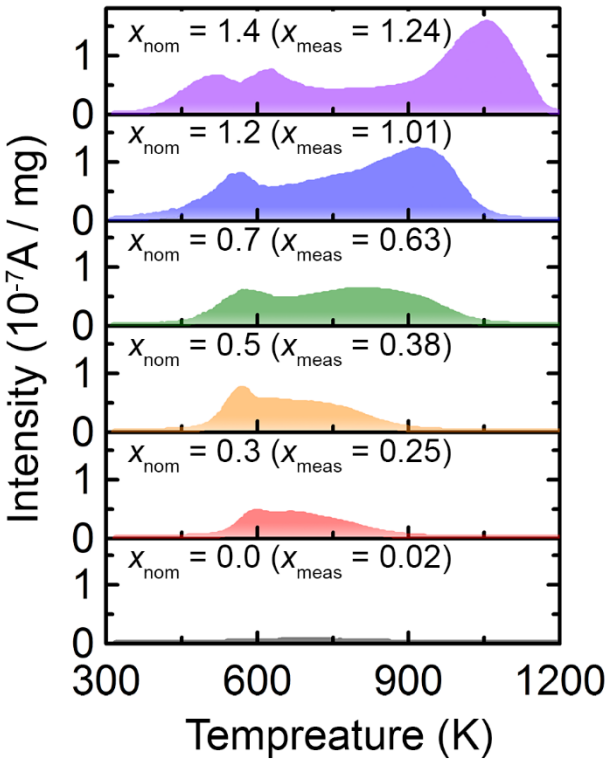

Figure 2-5. Thermal desorption spectrum (TDS) corresponding to the H_2 molecule (m/z = 2).

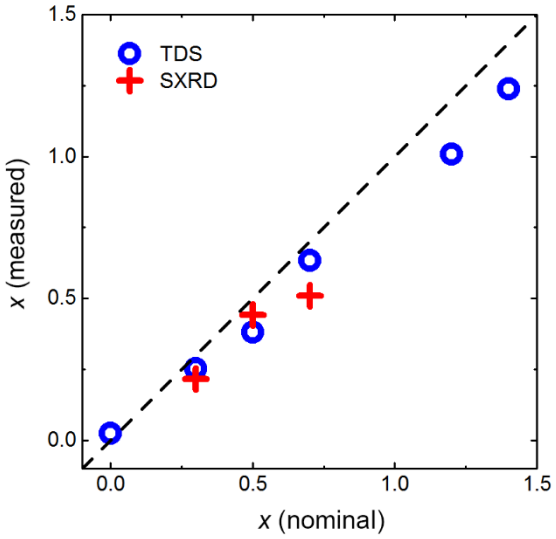

Figure 2-6. Hydrogen content measured by TDS data and oxygen vacancy estimated from synchrotron XRD data as a function of x_{nom}.

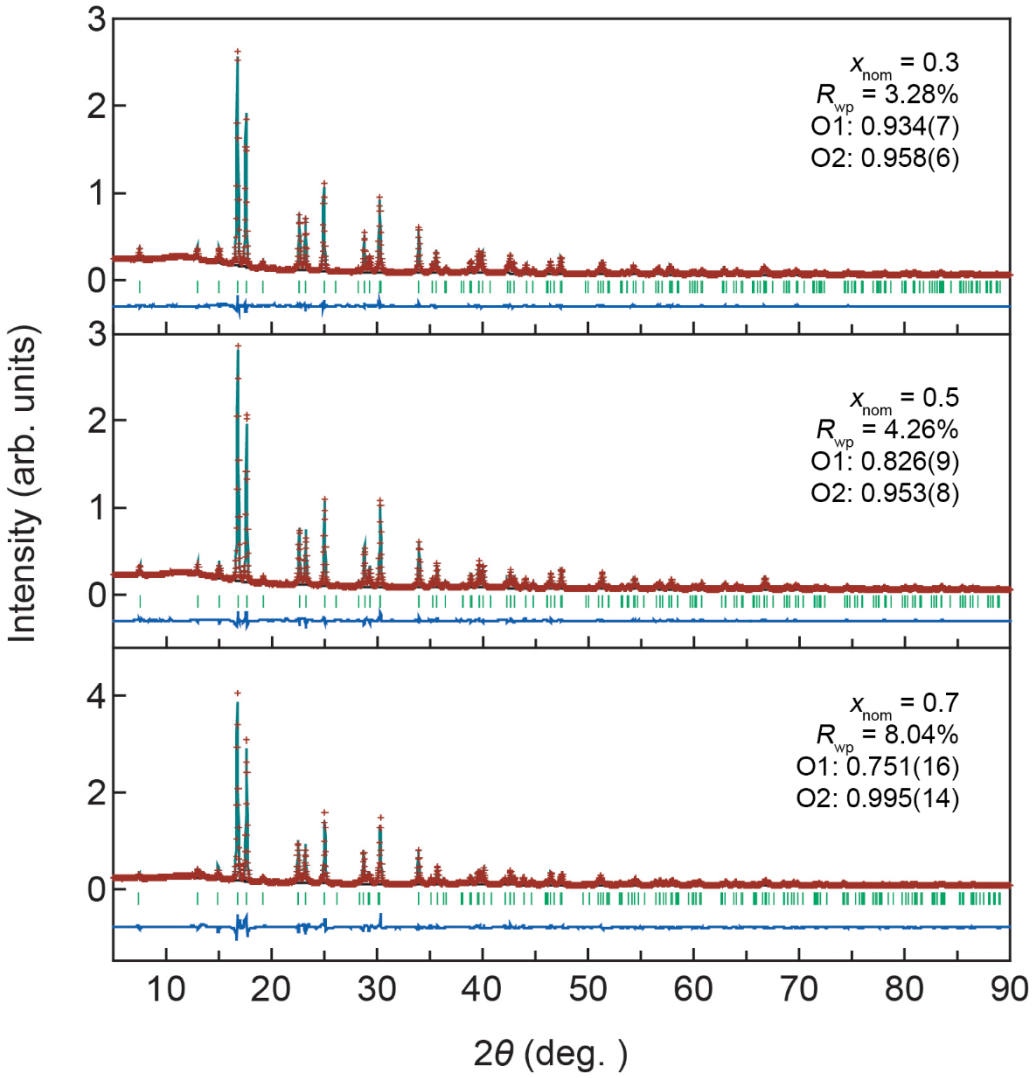

Figure 2-7. Rietveld fitting of synchrotron diffraction for $Sr_2VO_{4-x}H_x$ (x_{nom} = 0.3, 0.5, and 0.7, λ = 0.82722 Å).

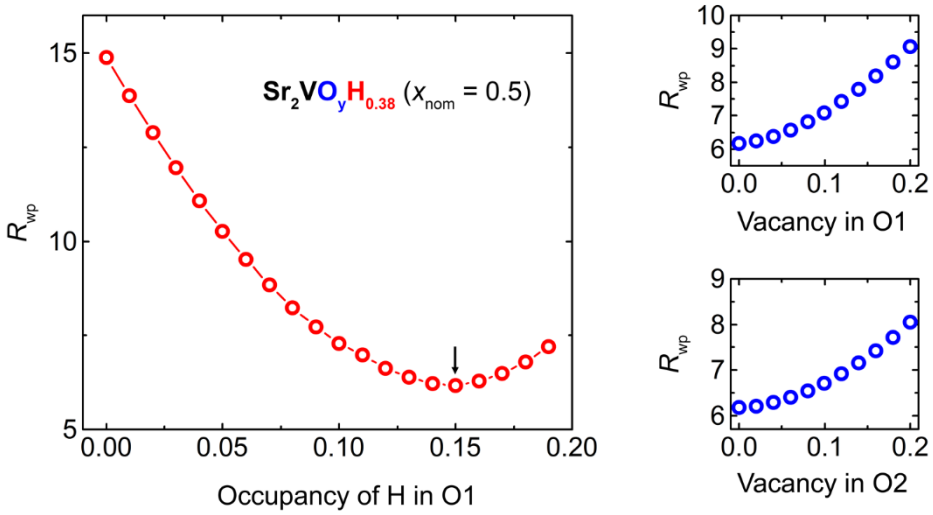

Figure 2-8. Residual factor of refinement R_{wp} for NPD data of $Sr_2VO_{4-x}H_x$ for x_{nom} = 0.5. Total amount of hydrogen is fixed to 0.38 for each pattern based on the TDS data. Right-hand side: R_{wp} for refinement of NPD patterns as a function of site occupancy for the each anion site. In this analysis, atomic parameters for each anion site, i.e., (x, y, z), B_{iso}, and hydrogen amount were fixed, whereas the site occupancy for the oxygen was treated as a parameter.

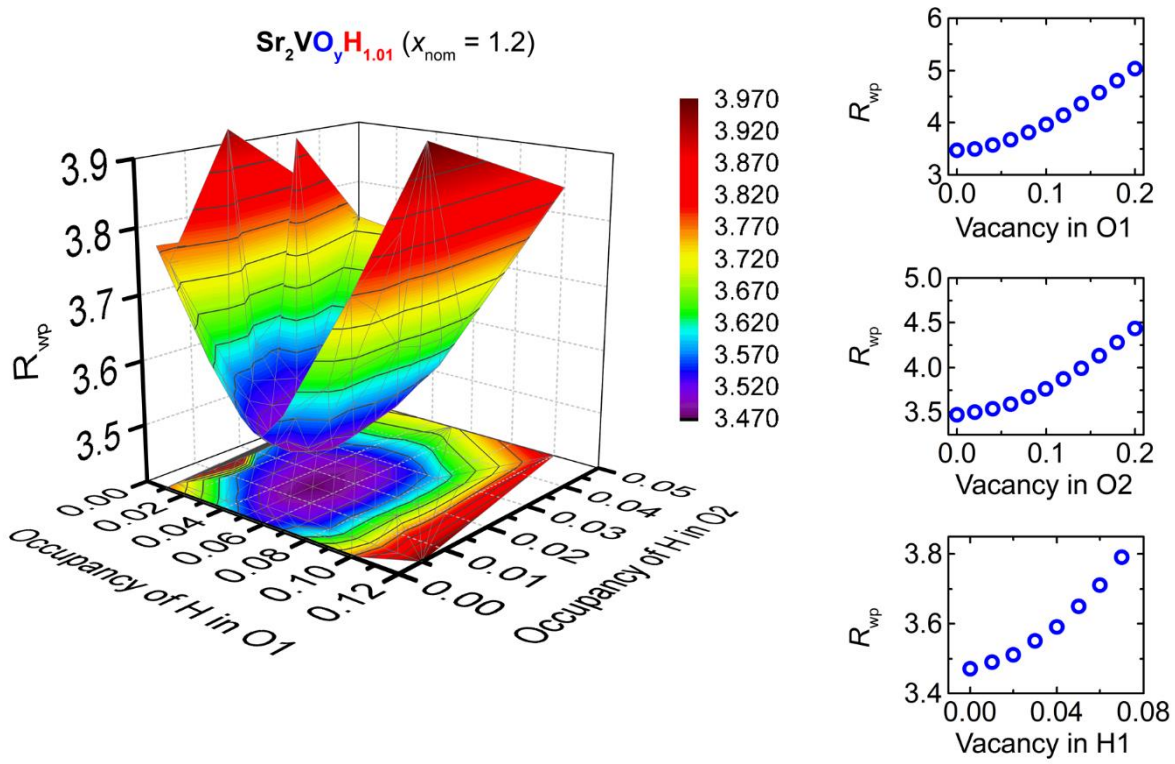

Figure 2-9. Residual factor of refinement R_{wp} for NPD data of $Sr_2VO_{4-x}H_x$ for x_{nom} = 1.2. Total amount of hydrogen is fixed to 1.01 for each pattern based on the TDS data. Right-hand side: R_{wp} for refinement of NPD patterns as a function of site occupancy for the each anion site. In this analysis, atomic parameters for each anion site, i.e., (x, y, z), B_{iso}, and hydrogen amount were fixed, whereas the site occupancy for the oxygen was treated as a parameter.

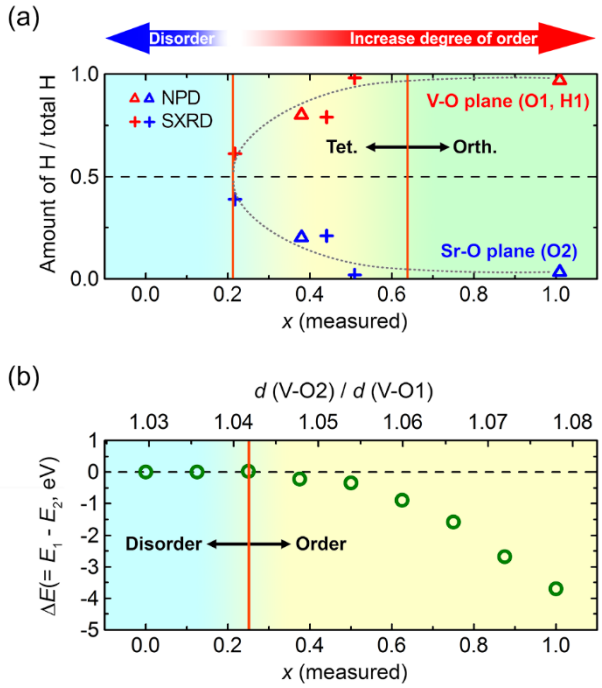

Figure 2-10. Anion order of $Sr_2VO_{4-x}H_x$ as a function of the H-substitution to oxygen sites. (a) Amount of hydrogen positioned in each plane derived by NPD and synchrotron XRD data. (b) Calculated total energy difference ($\Delta E = E_1 - E_2$) when hydrogen atoms occupy O1 (E_1) and O2 (E_2) sites in tetragonal $Sr_2VO_{4-x}H_x$.

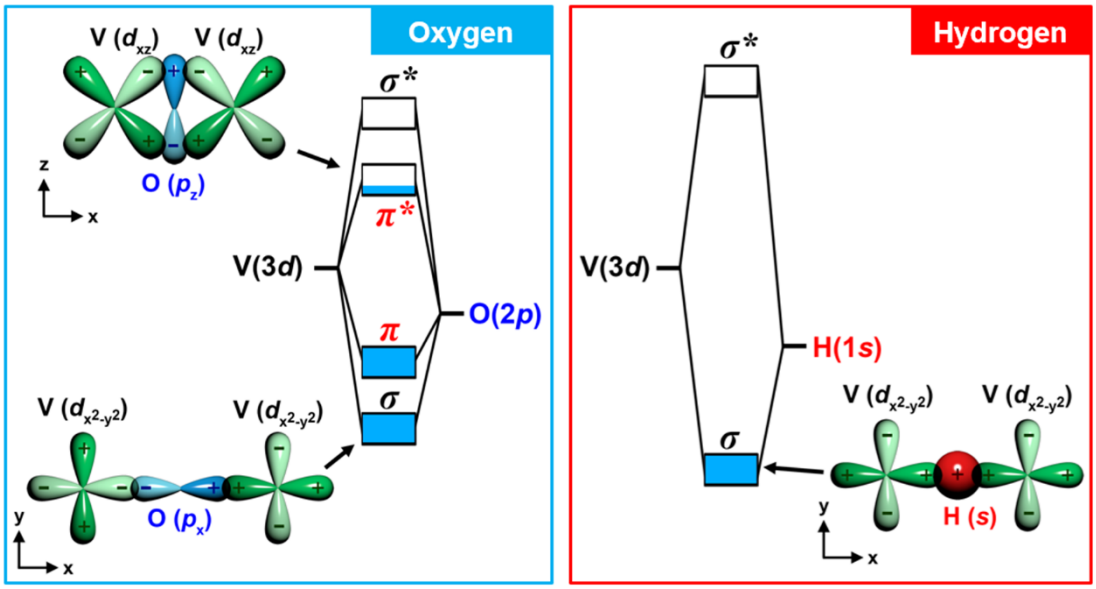

Figure 2-11. Schematic representation of molecular orbital diagram between vanadium cation and ligand anions (O, H).

Table 2-1. Lattice parameters of $Sr_2VO_{4-x}H_x$ (x_{nom}=0.0, 0.5, and 1.2) carried out by Rietveld fitting of NPD data.

Atom	Site	Occ.	*x*	*y*	*z*	B_{iso}(Å^2)
(a) $Sr_2VO_{3.92}$ (*I*4/*mmm*, *Z* = 2)						
a = 3.838083(78) Å, c = 12.555137(907) Å, V = 184.9483 Å^3, R_{wp} = 4.95						
$Sr_2VO_{4-x}H_x$ = 93.59%, SrO = 6.41%						
Sr	4e	1	0	0	0.355868(101)	0.547(28)
V	2a	1	0	0	0	0.237
O1	4c	0.989(4)	0	0.5	0	0.493(28)
O2	4e	0.969(4)	0	0	0.157426(110)	0.434(35)
(b) $Sr_2VO_{3.62}H_{0.38}$ (*I*4/*mmm*, *Z* = 2)						
a = 3.817189(83) Å, c = 12.671137(823) Å, V = 184.6303 Å^3, R_{wp} = 6.17						
$Sr_2VO_{4-x}H_x$ = 81.07%, SrO = 18.93%						
Sr	4e	1	0	0	0.353835(112)	0.550(22)
V	2a	1	0	0	0	0.237
O1	4c	O: 0.850 H: 0.150	0	0.5	0	0.398(22)
O2	4e	O: 0.960 H: 0.040	0	0	0.157719(125)	0.398(22)
(c) $Sr_2VO_{2.99}H_{1.01}$ (*Immm*, *Z* = 2)						
a = 3.681063(128) Å, b = 3.887802(117) Å, c = 12.783869(353) Å, V = 182.9531 Å^3, R_{wp} = 3.47						
$Sr_2VO_{4-x}H_x$ = 92.77%, SrO = 7.23%						
Sr	4i	1	0	0	0.351393(95)	0.495(22)
V	2a	1	0	0	0	0.237
O1	2d	O: 0.950 H: 0.050	0	0.5	0	0.183(37)
O2	4i	O: 0.985 H: 0.015	0	0	0.156735(125)	0.378(26)
H1	2b	O: 0.070 H: 0.930	0.5	0	0	1.693(95)

Chapter 3 Low Dimensionalization of Magnetic Ordering in a Transition-Metal Oxide by Hydride Ion Substitution

3.1 Introduction

Hydrogen is the most abundant element in the universe and it is also the simplest bipolar element. Recently, the hydride ion (H^-) has been of great interest in the solid-state community because of its unique electronic structure. Hydrogen has only one energetically available atomic orbital (the spherical 1*s* orbital), which is totally different from conventional anions such as oxygen and the halogens. It is expected that this unique electronic nature would provide the opportunity to realize novel physical properties in the compounds. In particular, I think utilization of hydride ion in *TM* oxides would be promising to emerge novel properties because the ionic radius of the hydride ion is similar to that of the oxide ion and there exists a distinct diversity in the chemical bonding by tuning the *d* electron count and available anion orbitals. Several *TM* oxyhydride compounds have been studied,[1–7] but the role of the hydride ion in the physical properties is still veiled.

In general, *TM* oxyhydrides have a perovskite structure with a 3*d TM* cation. In the case of simple perovskite-type oxyhydrides such as $ATiO_{3-x}H_x$ (*A* = Ca, Sr, and Ba),[4,5] oxygen and hydrogen are statistically located in equivalent anion sites. In contrast, in layered perovskite-type compounds such as $LaSrCoO_3H_{0.72}$,[1] there are non-equivalent anion sites and hydrogen and oxygen are isolated by different anion sites. In Chapter 2, compositionally tunable vanadium oxyhydrides, $Sr_2VO_{4-x}H_x$, were synthesized without accompanying the formation of

considerable anion vacancies.[6] It was found that hydrogen ordering and the corresponding structural transition with various O^{2-}/H^{-} contents using a combination of NPD, synchrotron XRD (SXRD), thermal desorption spectroscopy, and first-principles DFT calculations. In the low hydrogen substitution region ($x < 0.25$), hydrogen anions statistically occupy both anion sites in the V–O and Sr–O planes. With higher hydrogen substitution ($x > 0.25$), hydrogen anions tend to occupy the anion sites in the V–O planes. As more hydrogen is incorporated, the degree of anion order increases and finally most of hydrogen anions are located between the square-planes of oxide ions with a crystallographic phase transition (**Figure 2-4**). Romero et al. reported a checkerboard-type AFM ground state of Sr_2VO_3H with a Néel temperature (T_N) of ~170 K by a low-temperature neutron study and muon spin rotation (μSR) measurements **(Figure 3-1)**.[7]

Partial substitution of the oxide ion sites with hydride ions decreases the occupancy in the π-antibonding (π^*) molecular orbital with formation of strong σ bonds, which decreases the total energy of the crystal system. The extent of stabilization is more effective when hydrogen is located in the metal-oxide plane which anion site coordinated to two *TM* cations. Therefore, hydride ions are gradually ordered to the V–O planes with increasing hydrogen amount. Moreover, the *trans*-configuration of the hydride ion is stereochemically more stable than the *cis*-configuration, so hydride ions are finally located between the square-planes of oxide ions. This anion-ordered crystal structure is also found in the Co-based layered oxyhydride $LaSrCoO_3H_{0.72}$.[1] This type of hydrogen ordering forms two types of interaction pathways: *TM*–O–*TM* and *TM*–H–*TM*. Therefore, strong anisotropic behavior should be expected because of the different bonding nature between *TM* and O^{2-}/H^{-}.

In *TM* oxyhydrides, *TM* cations are octahedrally coordinated to both oxide ions with a $2p^6$ electronic configuration and hydride ions with a $1s^2$ configuration. Although the O 2*p* orbitals participate in both σ bonding with *TM* $d_{x^2-y^2}$ and d_{z^2} orbitals and π bonding with *TM* d_{xy}, d_{yz}, and d_{xz} orbitals, the H 1*s* orbital only participates in σ bonding with *TM* $d_{x^2-y^2}$ and d_{z^2} orbitals (**Figure 3-2**). The contribution of hydrogen to π bonding is negligible because the H 2*p* level is located ~10 eV above the H 1*s* level. For a localized spin system such as a Mott–Hubbard insulator, there is no significant overlap between *TM* cations. Therefore, the role of the "bridging" anion is important because the dominant part of the exchange interaction is a superexchange interaction through the intervening anion. In the case of the superexchange interaction, one key issue is the symmetry relation between the occupied *d* orbitals of the cation and the *p* or *s* orbitals of the anion.[8] From this point of view, a strong anisotropic exchange interaction can be achieved by the different orbital nature of the bridging anions, and low-dimensionality may be expected in anion-ordered oxyhydrides. This chapter demonstrates the role of the hydride ion in the physical dimensionality of *TM* compounds by showing the quasi-one-dimensional (1D) AFM spin-chain in the three-dimensional (3D) crystal structure of $Sr_2VO_{4-x}H_x$ with $x \sim 1$. Although understanding low-dimensionality in the *TM* oxide system is crucial for emerging novel physical properties ranging from high-temperature superconductors to spintronic devices, the magnetic dimensionality is generally restricted by the crystal structure (**Figure 3-3**)[9–12] because the exchange interaction strongly depends on the geometrical parameters, such as interatomic separation between magnetic ions. For this reason, utilization of hydride ions for emerging an anisotropic exchange interaction in 3D crystal structures provides a new idea for tuning the physical dimensionality in *TM* oxide systems.

3.2 Experimental details

Polycrystalline samples of $Sr_2VO_{4-x}H_x$ were synthesized by high-pressure solid-state reaction.[6] The temperature dependence of the DC electrical resistivity and the specific heat capacity were measured by the standard four-probe method and the thermal relaxation method using a physical property measurement system (PPMS, Quantum Design Inc., USA), respectively. The magnetic susceptibility was characterized using a magnetic property measurement system equipped with a superconducting quantum interference device–vibrating-sample magnetometer (MPMS SQUID-VSM, Quantum Design Inc., USA). Low-temperature long-range magnetic ordering was confirmed by μSR measurement using polycrystalline pellets. The μSR measurements were performed at the M15 surface-muon channel at TRIUMF (Vancouver, Canada). The SXRD measurements were performed using BL-8A at the KEK-PF.

3.3 Results and Discussion

Figure 3-4 shows the temperature-dependent magnetic susceptibility of $Sr_2VO_{4-x}H_x$. For x = 0.04, the χ (T) curve shows two anomalous points at 100 and 10 K (**Figure 3-4a**, inset), which are known as the orbital ordering[13] and magnetic transition (AFM ordering),[14] respectively. When H^- is introduced into the oxygen site, the magnetic susceptibility in the range 2–300 K increases with increasing x until x ~ 0.3, and then dramatically decreases until x = 1.00. The χ (T) curve of x = 1.00 (Sr_2VO_3H, $3d^2$) shows the lowest magnetic susceptibility throughout the whole temperature range. It was found that a small anomalous point at around 160 K, which is close to T_N (~170 K),[7] and magnetic suppression above 160 K with a large deviation from Curie–Weiss behavior (**Figure 3-4b**, inset). There is no significant difference between the zero-field cooling (ZFC) and field cooling (FC) curves. This magnetic behavior of Sr_2VO_3H is different from that reported in a previous study;[7] i.e., it shows the lack of both a signature related to AFM ordering and magnetic suppression above 160 K in the χ (T) curve with a considerable difference between the ZFC and FC curves. Considering that the magnetic susceptibility for x = 1.00 is about an order of magnitude smaller than the results in the previous study in the whole temperature range, these differences appear to arise from contamination of the secondary phases or a small deviation of the hydrogen content because of the different synthetic route. **Figure 3-5** shows the temperature-dependent electrical resistivity of polycrystalline $Sr_2VO_{4-x}H_x$. All of the samples show a positive slope with a linear relationship between log ρ and 1/T. Assuming that the electrical conductivity is caused by band electrons thermally excited across the band gap, the gap size is estimated to be 109 meV by Arrhenius fitting ($\rho = \rho_0 e^{-E_g/2k_BT}$). This is in good agreement with the Mott–Hubbard gap, that is, the

intersite *d–d* transition between vanadium cations in inelastic neutron[15] and optical studies.[16,17] In the first stage, E_g decreases to 96 meV with increasing x and then begins to increase up to 186 meV at $x = 0.50$ (**Figure 3-6**). For $x > 0.50$, E_g does not collapse and the samples show higher resistivity than our measurement range. The existence of an electrical band gap indicates that $Sr_2VO_{4-x}H_x$ is a localized spin system, therefore, increase of the effective magnetic moment (μ_{eff}) should be expected with increasing x. A Curie–Weiss fit to the magnetic susceptibility data in the high-temperature region (200–300 K) (**Figure 3-7**) gives the μ_{eff} value for each sample, as shown in **Figure 3-6**. Although μ_{eff} increases from 1.3 μ_B/V for $x = 0.04$ to 1.8 μ_B/V for $x = 0.31$, μ_{eff} starts to decrease from 1.8 μ_B/V for $x = 0.31$ to 0.3 μ_B/V for x =0.83. This trend coincides with the hydrogen ordering process; i.e., as hydride ions start to order into the V–O planes, the magnetic susceptibility is largely suppressed with increasing electrical band gap. Considering that the valence state of the vanadium cation in $Sr_2VO_{4-x}H_x$ changes from V^{4+} ($3d^1$) to V^{3+} ($3d^2$) with increasing x, suppression of the magnetic susceptibility is rather unusual. The ground state of Sr_2VO_3H ($3d^2$) shows AFM ordering (high-spin state, S = 1) and there is no structural transition, such as V–V dimerization (**Figure 3-8**). Thus, the possibility of spin crossover or the formation of the spin singlet is ruled out for this magnetic suppression.

Figure 3-9a shows the magnetic susceptibility curve of Sr_2VO_3H in the high-temperature region. The curve shows magnetic suppression with a broad maximum (T_{max} = 382 K) which appears to be a specific feature of 1D AFM spin-chain systems.[11,18–30] As the temperature decreases, the magnetic susceptibility is gradually suppressed from 382 K and shows a large deviation from Curie–Weiss behavior. As shown in **Figure 3-9c**, the observed muon spin

oscillation frequencies (ν) are consistent with the magnetic suppression of ~160 K in the $\chi(T)$ curve, and the magnetic moment is estimated to be 2.13 μ_B per vanadium atom, which is reasonable value for a V^{3+} ion with a $3d^2$ electron configuration. The nonmagnetic volume fraction (f_p) gradually decreases from 180 to 120 K (ΔT ~ 60 K) and f_p at 2 K is only 0.14. Even though magnetic suppression appears in the $\chi(T)$ curve, no magnetic ordering signal is present above 180 K in the μSR data, which suggests the formation of short-range AFM ordering, such as a 1D Heisenberg antiferromagnet (1D-HAF) spin-chain system. The observed upturn in the low-temperature region, which is common for quasi-1D magnetic systems,[11,24–26,29,31,32] possibly originates from the Curie–Weiss contribution arising from finite length chains and/or paramagnetic impurities.

The $\chi(T)$ curve above T_N was fitted using the S = 1 1D-HAF spin-chain model with the following equation:[20,21]

$$\chi_{spin} = \frac{Ng^2\mu_B^2}{k_BT}\left[\frac{2 + 0.0194x + 0.777x^2}{3 + 4.346x + 3.232x^2 + 5.834x^3}\right], \quad (1)$$

where $x = |J|/k_BT$ and g = 2.00. To fit the susceptibility data, It is assumed that the observed susceptibility consists of three terms:[24,25]

$$\chi(T) = \chi_0 + (1 - f)(\chi_{\mathrm{spin}}) + f(\chi_{\mathrm{CW}}), \quad (2)$$

where χ_0 is the temperature-independent term including the diamagnetic contribution of the ion core, χ_{spin} is the spin contribution of the V^{3+} ions, and χ_{CW} is a Curie–Weiss component arising from finite length chains and/or paramagnetic impurities. The experimental curve fits well (standard deviation $\chi^2 = 2.376 \times 10^{-13}$) to the 1D-HAF model (red dashed line), with $\chi_0 = -3.316 \times 10^{-4}$ emu/mol V and exchange coupling constant $J = -29.1$ meV ($|J|/k_B = 338$ K, $|J|/T_{max} \sim 0.88$). The contribution of the Curie–Weiss component is 3.4% ($f = 0.034$) and the Curie–Weiss temperature $\theta = -18$ K.

Assuming that the origin of the Curie–Weiss contribution is the paramagnetic impurity phase containing V^{3+} or V^{4+} ions, the secondary phase corresponding to 3.4 or 9.1 mol.% of the total V ions should be detected by NPD measurement. However, such a significant amount of magnetic impurities was not observed in the Sr_2VO_3H sample (Sr_2VO_3H = 93 wt.% and SrO = 7 wt.%).[6] Therefore, the finite length chain effect in the main phase is more likely to be the cause of the Curie–Weiss contribution.[24] **Figure 3-9b** shows the temperature-dependent spin susceptibility (χ_{spin}) curve of Sr_2VO_3H with the theoretical curves by $S = 1$ 1D-HAF model for various values of J. When $T > T_N$, χ_{spin} is reproduced well by the 1D-HAF model with $J = 338$ K, while significant deviation from the theoretical model was found below T_N where long-range AFM ordering develops.

The inset of **Figure 3-9a** shows the temperature dependence of the heat capacity. The λ-shaped magnetic heat-capacity (C_p) peak usually associated with the paramagnetic to AFM transition is not observed with and without an external magnetic field (H = 0 and 7 T). This heat capacity behavior is consistent with a 1D Heisenberg spin-chain system;[18,33–35] i.e., drastic entropy loss does not occur at T_N because most of the magnetic entropy above T_N is lost because

of the enhanced spin fluctuation by 1D short-range magnetic ordering.

3.4 Conclusion

In this chapter, magnetic low-dimensionalization in Sr_2VO_4 was discussed. By substituting O^{2-} with H^-, low-dimensionalization of magnetic ordering was realized in a *TM* oxide Sr_2VO_4. Upon increasing x in $Sr_2VO_{4-x}H_x$, the hydride ions were ordered linearly, and the magnetic susceptibility was simultaneously suppressed above the Néel temperature (160 K). Formation of short-range AFM ordering was found by a combination of μSR and magnetic susceptibility data. The magnetic susceptibility curve shows magnetic suppression with a broad maximum (T_{max} = 382 K), which is a specific feature of 1D AFM spin-chain systems. By comparing the experimental data with a 1D-HAF spin-chain model, it was found that this magnetic behavior was attributed to the formation of a quasi-1D AFM spin-chain with exchange coupling constant $J \sim -29$ meV.

References

1. M. A. Hayward, E. J. Cussen, J. B. Claridge, M. Bieringer, M. J. Rosseinsky, C. J. Kiely, S. J. Blundell, I. M. Marshall, and F. L. Pratt, Science 295, 1882 (2002).

2. K. Poeppelmeier, Science 295, 1849 (2002).

3. R. M. Helps, N. H. Rees, and M. A. Hayward, Inorg. Chem. 49, 11062 (2010).

4. Y. Kobayashi, O. J. Hernandez, T. Sakaguchi, T. Yajima, T. Roisnel, Y. Tsujimoto, M. Morita, Y. Noda, Y. Mogami, A. Kitada, M. Ohkura, S. Hosokawa, Z. Li, K. Hayashi, Y. Kusano, J. Kim, N. Tsuji, A. Fujiwara, Y. Matsushita, K. Yoshimura, K. Takegoshi, M. Inoue, M. Takano, and H. Kageyama, Nat. Mater. 11, 507 (2012).

5. T. Sakaguchi, Y. Kobayashi, T. Yajima, M. Ohkura, C. Tassel, F. Takeiri, S. Mitsuoka, H. Ohkubo, T. Yamamoto, J. Kim, N. Tsuji, A. Fujihara, Y. Matsushita, J. Hester, M. Avdeev, K. Ohoyama, and H. Kageyama, Inorg. Chem. 51, 11371 (2012).

6. J. Bang, S. Matsuishi, H. Hiraka, F. Fujisaki, T. Otomo, S. Maki, J.-I. Yamaura, R. Kumai, Y. Murakami, and H. Hosono, J. Am. Chem. Soc. 136, 7221 (2014).

7. F. Denis Romero, A. Leach, J. S. Möller, F. Foronda, S. J. Blundell, and M. A. Hayward, Angew. Chemie 126, 7686 (2014).

8. J. Kanamori, J. Phys. Chem. Solids 10, 87 (1959).

9. M. T. Hutchings, G. Shirane, R. J. Birgeneau, and S. L. Holt, Phys. Rev. B 5, 1999 (1972).

10. I. U. Heilmann, G. Shirane, Y. Endoh, R. J. Birgeneau, and S. L. Holt, Phys. Rev. B 18,

3530 (1978).

11. W. E. Estes, D. P. Gavel, W. E. Hatfield, and D. J. Hodgson, Inorg. Chem. 17, 1415 (1978).

12. R. M. Morra, W. J. L. Buyers, R. L. Armstrong, and K. Hirakawa, Phys. Rev. B 38, 543 (1988).

13. H. D. Zhou, B. S. Conner, L. Balicas, and C. R. Wiebe, Phys. Rev. Lett. 99, 136403 (2007).

14. J. Sugiyama, H. Nozaki, I. Umegaki, W. Higemoto, E. J. Ansaldo, J. H. Brewer, H. Sakurai, T.-H. Kao, H.-D. Yang, and M. Månsson, Phys. Rev. B 89, 020402 (2014).

15. H. D. Zhou, Y. J. Jo, J. Fiore Carpino, G. J. Munoz, C. R. Wiebe, J. G. Cheng, F. Rivadulla, and D. T. Adroja, Phys. Rev. B 81, 212401 (2010).

16. J. Matsuno, Y. Okimoto, M. Kawasaki, and Y. Tokura, Phys. Rev. Lett. 95, 176404 (2005).

17. J. Matsuno, Y. Okimoto, M. Kawasaki, and Y. Tokura, Appl. Phys. Lett. 82, 194 (2003).

18. J. C. Bonner and M. E. Fisher, Phys. Rev. 135, A640 (1964).

19. W. E. Estes, R. R. Weller, and W. E. Hatfield, Inorg. Chem. 19, 26 (1980).

20. A. Meyer, A. Gleizes, J. J. Girerd, M. Verdaguer, and O. Kahn, Inorg. Chem. 21, 1729 (1982).

21. V. Gadet, M. Verdaguer, V. Briois, A. Gleizes, J. P. Renard, P. Beauvillain, C. Chappert,

T. Goto, K. Le Dang, and P. Veillet, Phys. Rev. B 44, 705 (1991).

22. M. Hase, I. Terasaki, and K. Uchinokura, Phys. Rev. Lett. 70, 3651 (1993).

23. S. Eggert, I. Affleck, and M. Takahashi, Phys. Rev. Lett. 73, 332 (1994).

24. T. Ami, M. K. Crawford, R. L. Harlow, Z. R. Wang, D. C. Johnston, Q. Huang, and R. W. Erwin, Phys. Rev. B 51, 5994 (1995).

25. N. Motoyama, H. Eisaki, and S. Uchida, Phys. Rev. Lett. 76, 3212 (1996).

26. J. L. Dye, Inorg. Chem. 36, 3816 (1997).

27. R. H. Huang, M. J. Wagner, D. J. Gilbert, K. A. Reidy-Cedergren, D. L. Ward, M. K. Faber, and J. L. Dye, J. Am. Chem. Soc. 119, 3765 (1997).

28. K. Fabricius, A. Klümper, U. Löw, B. Büchner, T. Lorenz, G. Dhalenne, and A. Revcolevschi, Phys. Rev. B 57, 1102 (1998).

29. T. Masuda, T. Sakaguchi, and K. Uchinokura, J. Phys. Soc. Japan 71, 2637 (2002).

30. H. H. Ko, J. H. Lim, H. C. Kim, and C. S. Hong, Inorg. Chem. 45, 8847 (2006).

31. E. E. Kaul, H. Rosner, V. Yushankhai, J. Sichelschmidt, R. V. Shpanchenko, and C. Geibel, Phys. Rev. B 67, 174417 (2003).

32. M. D. Johannes, J. Richter, S.-L. Drechsler, and H. Rosner, Phys. Rev. B 74, 174435 (2006).

33. L. J. De Jongh and A. R. Miedema, Adv. Phys. 50, 947 (2010).

34. M. D. Chabot and J. T. Markert, Phys. Rev. Lett. 86, 163 (2001).

35. K. Kudo, S. Kurogi, Y. Koike, T. Nishizaki, and N. Kobayashi, Phys. Rev. B 71, 104413 (2005).

Figures

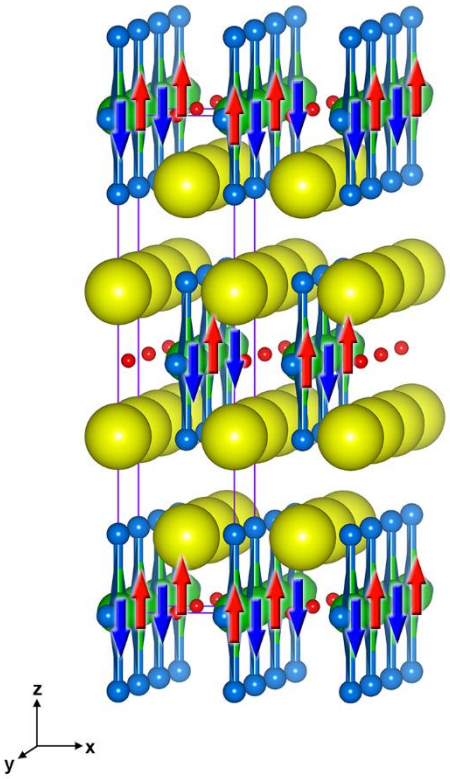

Figure 3-1. Checkerboard-type AFM ordering of Sr_2VO_3H from NPD data.

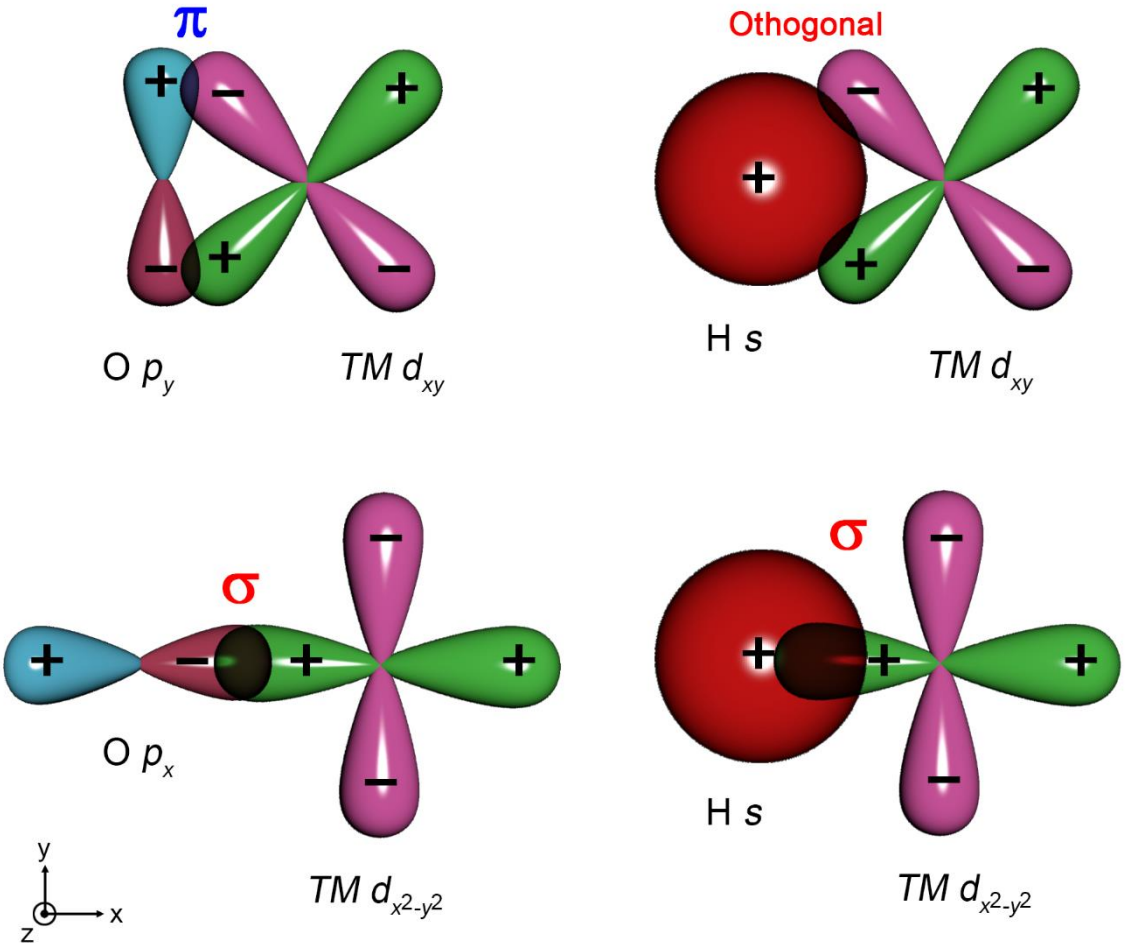

Figure 3-2. Symmetry relation of *TM* 3*d* and O 2*p*/H 1*s* orbitals.

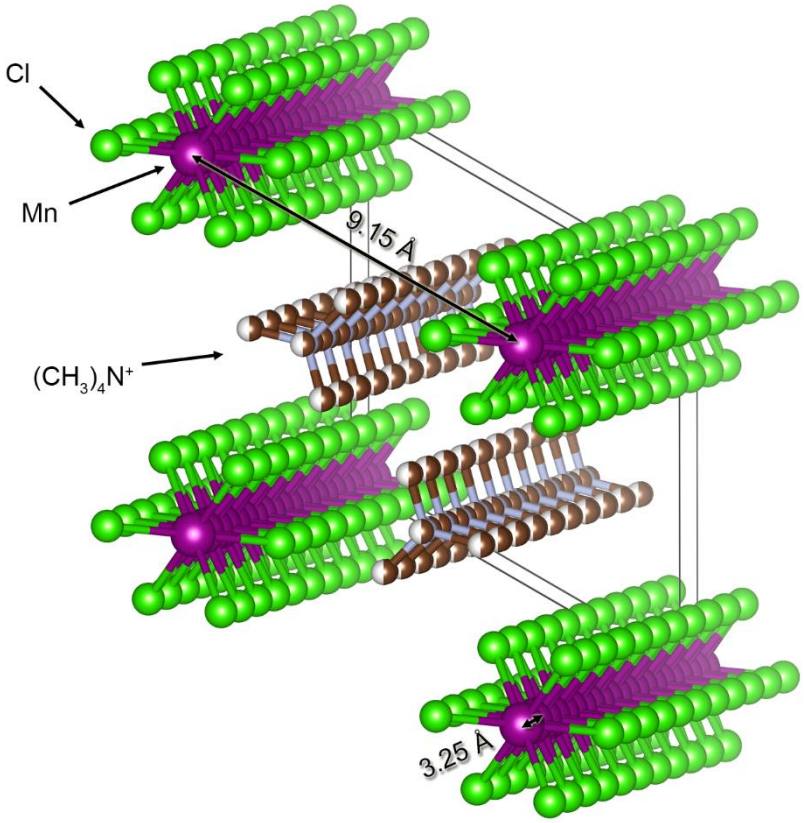

Figure 3-3. Crystal structure of $(CH_3)_4NMnCl_3$. This structure has space group *P*63/*m* with the $(CH_3)_4N^+$ ions statistically disordered relative to the crystal *c* axis.

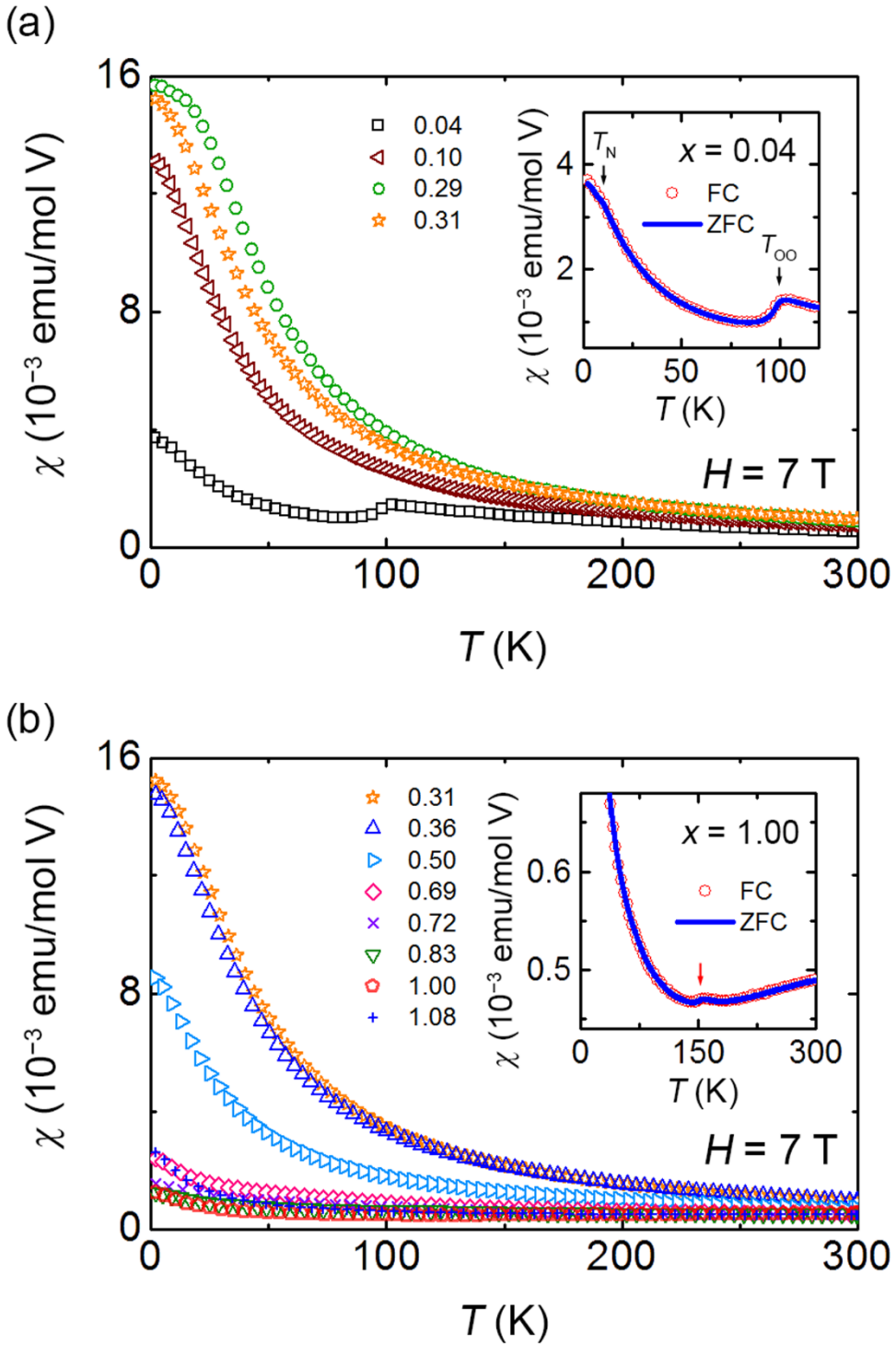

Figure 3-4. Temperature-dependent magnetic susceptibility when H = 7 T. The inset shows the zero-field cooled (ZFC) and field cooled (FC) magnetic susceptibilities for x = 0.04 and 1.00.

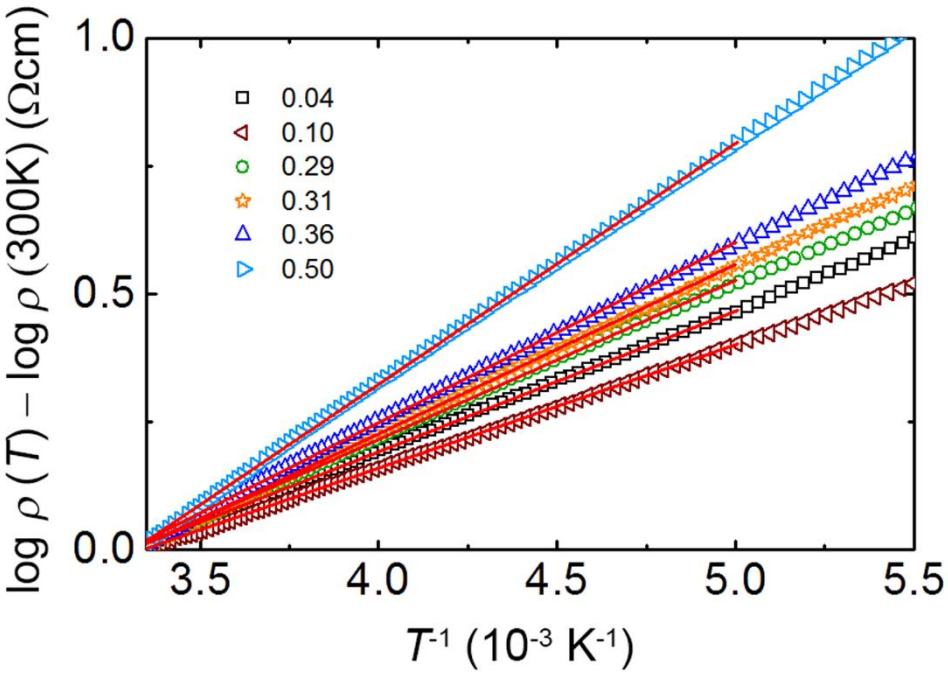

Figure 3-5. Temperature-dependent electrical resistivity data and their Arrhenius fit (red line) in the range 200–300 K. For $x > 0.50$, the resistivity of each sample is beyond the range of our measurement system.

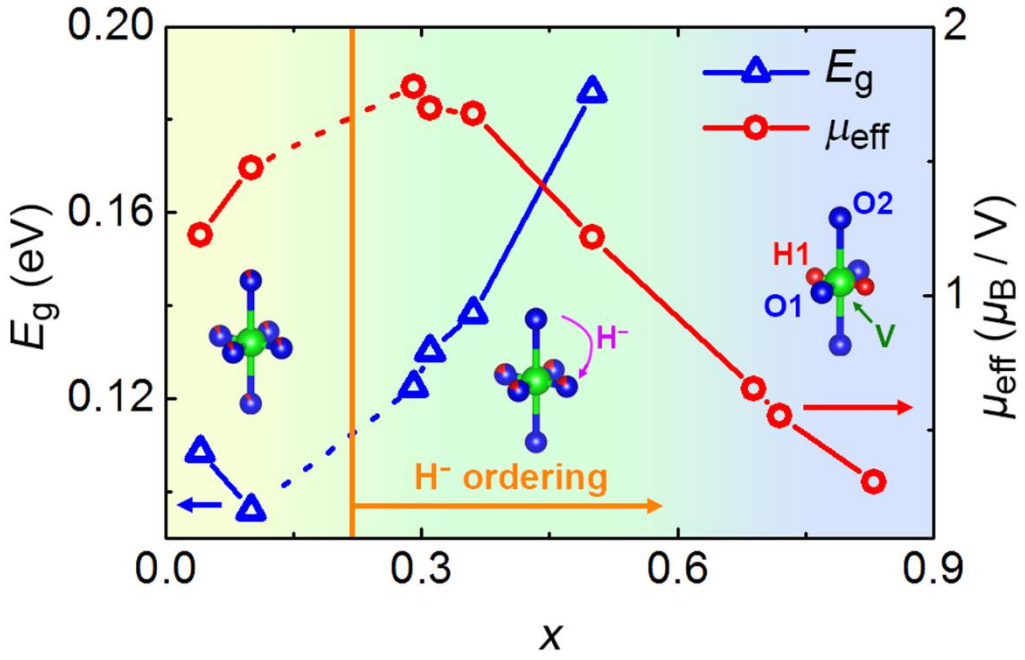

Figure 3-6. Electrical band gap (E_g) and effective magnetic moment (μ_{eff}) as a function of x. Hydrogen anions statistically occupy each oxygen anion site in the low hydrogen substitution region ($x < 0.25$) and are gradually ordered in the V–O plane with increasing hydrogen content and aA crystallographic transition (tetragonal to orthorhombic) occurs between $x = 0.50$ and 0.69.

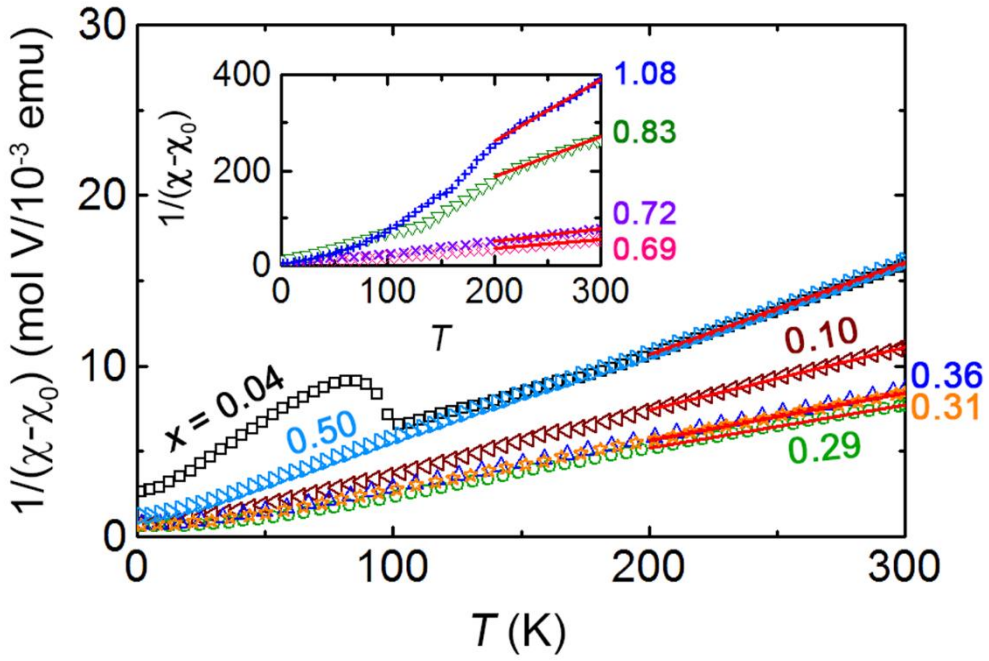

Figure 3-7. Inverse susceptibility ($1/(\chi-\chi_0)$) curves of $Sr_2VO_{4-x}H_x$. Red lines show Curie–Weiss fitting in the range 200–300 K.

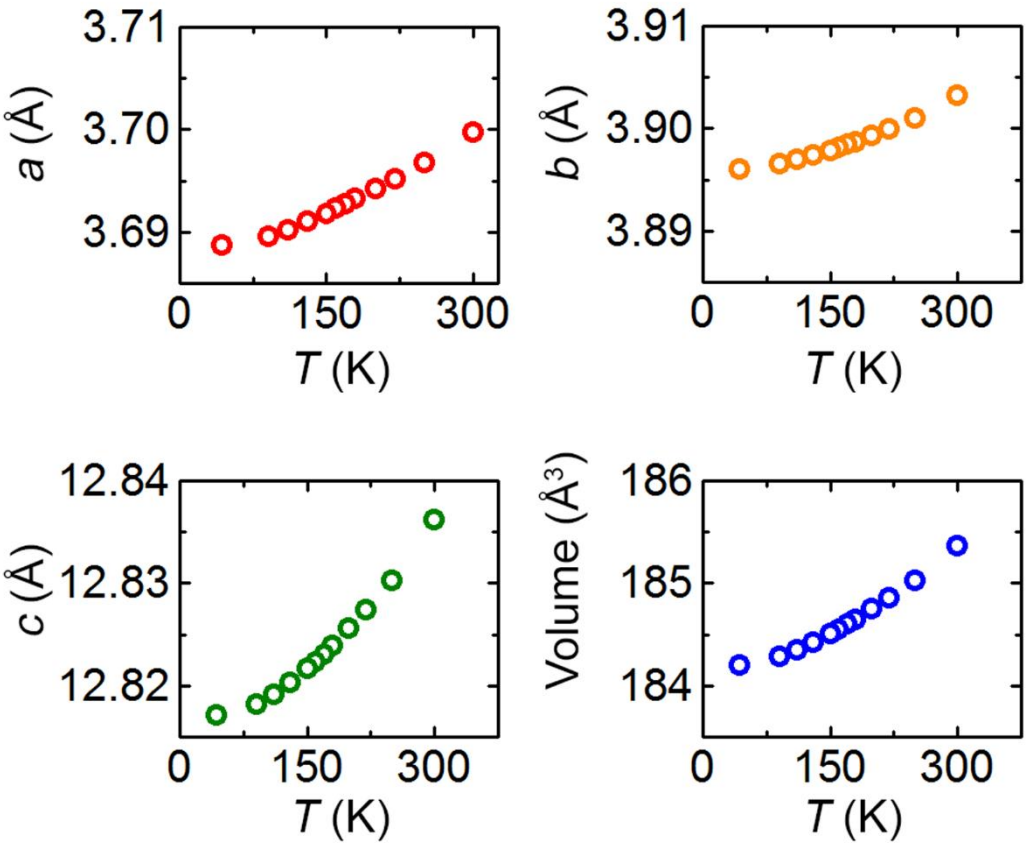

Figure 3-8. Temperature-dependent lattice parameters *a*, *b*, and *c*, and volume of Sr_2VO_3H obtained by SXRD.

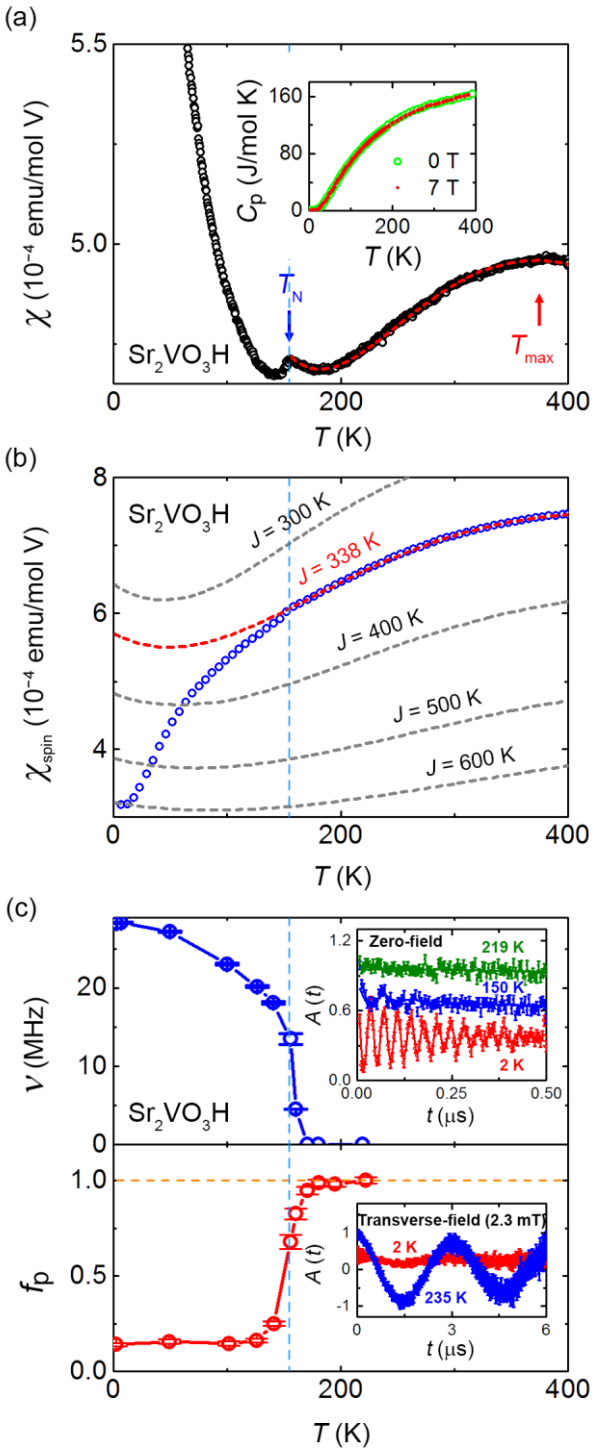

Figure 3-9. Low-dimensional behavior of Sr_2VO_3H. (a) Temperature-dependent magnetic susceptibility of Sr_2VO_3H (x = 1.00) in the high-temperature region. The red dashed curve shows the theoretical trace of the 1D-HAF spin-chain system including 3.4% Curie–Weiss component (χ_{CW}). The inset shows the temperature-dependent heat capacity (C_p) data for Sr_2VO_3H with/without an external magnetic field (0 and 7 T). (b) Spin susceptibility (χ_{spin}) for Sr_2VO_3H (blue open circles) and the theoretical curves (dashed lines) of the S = 1 1D-HAF spin-chain model for various exchange coupling constants J. (c) Temperature-dependent muon spin oscillation frequencies (ν) and nonmagnetic volume fraction (f_p) for Sr_2VO_3H. The inset shows zero- and transverse-field time spectra of Sr_2VO_3H at various temperatures.

Chapter 4 Anisotropic Exchange Interaction in Transition-Metal Oxyhydrides by the Isotropic Electronic Structure of the H 1*s* Orbital

4.1 Introduction

Understanding the interplay between orbital, spin, and charge degrees of freedom in solids is one of the goals of condensed matter physics. In *TM* compounds, the spin degree of freedom is strongly affected by the exchange interactions between magnetic ions. The dimensionality of the physical system can restrict the interaction pathway, and therefore plays an important role in the magnetic properties of the material. In general, the dimensionality is predetermined by the crystal structure because the exchange interaction strongly depends on geometrical parameters, such as the interatomic separation between magnetic ions. For this reason, 1D magnetic behavior is generally observed for systems with a linear-chain crystal structure, which shows the large spatial anisotropy between magnetic ions.[1–5]

Considering the important role of bridging anions, which mediate electronic and magnetic interaction between magnetic ions, the physical dimensionality can be tuned by changing the intervening anion. The hydride ion has spherical symmetry of the 1*s* orbital, which is totally different from other ligand anion such as N^{3-}, O^{2-}, F^{-} and Cl^{-}, in which the anisotropic 2*p* orbital is energetically available. Therefore, a large anisotropic exchange interaction can be achieved by the different orbital nature of the bridging anions, and low dimensionality is expected in anion-ordered oxyhydrides.[6,7]

In Chapter 3, low-dimensional magnetic behavior of compositionally tunable $Sr_2VO_{4-x}H_x$

vanadium oxyhydrides was observed. Although the physical properties of $Sr_2VO_{4-x}H_x$ indicate that low-dimensionality should be related to hydride ion ordering, a detailed explanation of the origin of the low-dimensionality is not available. In this chapter, DFT calculations were performed to investigate the origin of the 1D magnetic behavior in *TM* oxyhydrides $Sr_2VO_{4-x}H_x$.

4.2 Computational methods

DFT calculations were performed using the experimental crystallographic parameters within the full-potential linearized augmented-plane-wave method implemented in the WIEN2k package.[8,9] The general gradient approximation (GGA)[10] was used for the exchange–correlation potential with on-site repulsion (U). The product of the muffin-tin radius (R_{MT}) and the largest wavenumber of the basis set (K_{max}) was fixed at 6.0, and the charge density was Fourier expanded up to G_{max} = 20 Bohr^{-1}. The following R_{MT} values were employed: $R_{MT\text{-}Sr}$ = 2.34 Bohr, $R_{MT\text{-}V}$ = 1.92 Bohr, $R_{MT\text{-}O}$ = 1.73 Bohr, and $R_{MT\text{-}H}$ = 1.21 Bohr. Self-consistency was carried out for four types of spin-ordered states using a $2a \times 2b \times c$ supercell containing 56 atoms, and a $6 \times 6 \times 12$ k-point mesh was used. The energy convergence was set to 10^{-6} Ry for self-consistency. To calculate the hopping integral between V and O, and V and H orbitals, the maximally localized Wannier functions (MLWFs) for V 3d, O 2p, and H 1s orbitals were constructed (**Table 4-1**) using the WANNIER90[11] and WIEN2WANNIER[12] codes.

4.3 Results and Discussion

To investigate the origin of the magnetic low-dimensionalization, the four types of spin-ordered states are constructed shown in **Figure 4-1** and calculated the spin-exchange coupling constants for three exchange interaction pathways using the Ising spin Hamiltonian:

$$\hat{H} = -\sum_{i<j} J_{ij}\hat{S}_{iz}\hat{S}_{jz}, \tag{3}$$

where J_{ij} is the spin-exchange coupling parameter between spin sites i and j, and $\hat{S}_{iz}$ and $\hat{S}_{jz}$ are the operators for the z components of the spin angular momentum at spin sites i and j, respectively. The total energy differences between these spin-ordered states for various on-site Hubbard interactions U (1.5–4.5 eV) and the resultant exchange coupling constants J are summarized in **Table 4-2**. For each U, the AFM1 model gave the lowest total energy, which is in agreement with the experimental observations. Another important result is that the total energy difference between the AFM1 and AFM3 models is quite small, while the total energy of the AFM2 model is much higher than that of the AFM3 model, and it is similar to the total energy of the FM model. These results indicate that the AFM spin configuration along the V–O–V direction is energetically more stable than the FM spin configuration regardless of the spin configuration along the V–H–V direction; i.e., the formation of a 1D AFM spin-chain along V–O–V is energetically stable while the interchain exchange interaction is not dominant in determining the magnetic stability. Both the V–O–V (J_1) and V–H–V (J_2) exchange

interactions show AFM interactions (negative J), and there is a large anisotropy between the two exchange energies, with a J_1/J_2 ratio of ~6 for the different values of U. These results indicate that the AFM superexchange interaction between vanadium cations through the oxide ion is much stronger than that through the hydride ion. Although the interatomic distance between vanadium cations in V–H–V (3.68 Å) is shorter than that in V–O–V (3.89 Å), the value of J_1 is six times larger, indicating that the superexchange interaction strongly relies on the identity of the intervening anion, not the spatial distance, in the present case.

As previously mentioned, the symmetric relationship between magnetic ions and bridging anions plays an important role in the superexchange interaction between magnetic ions. **Table 4-3** shows the hopping integrals between V 3*d* and O 2*p*/H 1*s* orbitals using MLWFs based on the results of a GGA+*U* calculation (**Figure 4-2** and **Figure 4-3**). For an oxide ion in the V–O planes (O1, see the crystal structure in **Figure 4-1a**), hopping is dominant between V d_{xy} and O p_x, V d_{yz} and O p_z, and V $d_{x^2-y^2}$ and O p_y orbitals, which form d–p π- and d–p σ-exchange interactions. In contrast, for a hydride ion, hopping between H s and V d_{z^2} orbitals is dominant, which gives rise to only the d–s σ-exchange interaction. The hopping integral of d–s σ-bonding for a hydride ion is 2.2 eV, which is larger than that of d–p σ-bonding for an oxide ion (1.7–1.8 eV), and d–p π-bonding for an oxide ion has the smallest value of ~1 eV. This result is reasonable because the exchange interaction of σ bonding is stronger than that of π bonding and the interatomic distance between V and H is shorter than that of V and O. Considering the stronger hopping integral between H 1*s* and V 3*d* orbitals than between O 2*p* and V 3*d* orbitals, the superexchange interaction along the V–H–V direction seems to be stronger than that along the V–O–V direction, which is the opposite conclusion from the calculated exchange

interaction. However, the orbital occupancy should be considered because the exchange interaction strongly depends on the occupancy of the interacting orbitals.

Figure 4-4 shows the total and partial density of states (DOSs) for Sr_2VO_3H. The partial density of states (PDOSs) show the energy overlap of relevant orbitals that participate in π- and σ-exchange interactions, which is consistent with the results of the hopping integrals in **Table 4-3**. By calculating the spin occupancy for each V *d* orbital, It was found that most unpaired spins are occupied in the V d_{xz} (48.1%) and d_{yz} (45.4%) orbitals, and only a small portion are distributed in the V d_{z^2} (2.5%) and V $d_{x^2-y^2}$ (1.9%) orbitals as shown in **Table 4-3**. This finding means that most unpaired spins are associated with the π-exchange interaction with the oxide ion along the V–O–V chain direction, and only a small portion of unpaired spins participate in the σ-exchange interaction with oxide and hydride ions. Therefore, anisotropic superexchange interactions are formed and a 1D AFM spin-chain developed along the V–O–V direction despite the larger σ-hopping strength between V and H because the spherical *s* orbital of the hydride ion is orthogonal to the V d_{xy}, d_{yz}, and d_{xz} orbitals, as shown in **Figure 4-5**. These results suggest a new approach for tuning the physical dimensionality using heteromorphic mixed anions which is totally different from the conventional route, that is, control of the orbital overlap between neighboring ions.

4.4 Conclusion

In this chapter, the origin of magnetic low-dimensionalization was investigated using first principles calculations. Formation of a quasi-1D AFM spin-chain occurred through the second nearest neighbor of the vanadium cation with hydrogen ordering in $Sr_2VO_{4-x}H_x$ with $x = 1$. Substitution of a hydride ion for an oxide ion can break the π-exchange interaction between the *TM* ion and the oxide ion, causing an anisotropic exchange interaction. In the case of early *TM* oxides in which only the d_{xy}, d_{yz}, and d_{xz} orbitals are occupied, the absence of an exchange pathway through *TM*–H–*TM* can introduce low-dimensionalization in the 3D crystal structure when the substituted hydride ions are ordered low-dimensionally. For *TM* oxides with electrons occupying the $d_{x^2-y^2}$ and d_{z^2} orbitals, the σ-exchange interaction through *TM*–H–*TM* works effectively, so the low dimensionalization effect described above is negligible. Thus, we may understand the strong AFM ordering ($T_N > 350$ K)[1] reported for Co-based oxyhydrides by the high occupation of unpaired spins in $d_{x^2-y^2}$ and d_{z^2} orbitals, which forms the strong superexchange interaction through the Co–H–Co pathway in addition to the Co–O–Co pathway. The present finding indicates the possibility achieving novel electronic and magnetic behavior of *TM* compounds by utilizing heteromorphic mixed anions.

References

1. M. Hutchings, G. Shirane, R. Birgeneau, and S. Holt, Phys. Rev. B **5**, 1999 (1972).
2. I. U. Heilmann, G. Shirane, R. J. Birgeneau, and S. L. Holt, Phys. Rev. B **18**, 3530 (1978).
3. W. J. L. Buyers, R. M. Morra, R. L. Armstrong, M. J. Hogan, P. Gerlach, and K. Hirakawa, Phys. Rev. Lett. **56**, 371 (1986).
4. M. Hase, I. Terasaki, and K. Uchinokura, Phys. Rev. Lett. **70**, 3651 (1993).
5. N. Motoyama, H. Eisaki, and S. Uchida, Phys. Rev. Lett. **76**, 3212 (1996).
6. M. A. Hayward, E. J. Cussen, J. B. Claridge, M. Bieringer, M. J. Rosseinsky, C. J. Kiely, S. J. Blundell, I. M. Marshall, and F. L. Pratt, Science 295, 1882 (2002).
7. J. Bang, S. Matsuishi, H. Hiraka, F. Fujisaki, T. Otomo, S. Maki, J. Yamaura, R. Kumai, Y. Murakami, and H. Hosono, J. Am. Chem. Soc. 136, 7221 (2014).
8. P. Blaha, K. Schwarz, G. K. H. Madsen, D. Kvasnicka and J. Luitz, WIEN2k, An Augmented Plane Wave + Local Orbitals Program for Calculating Crystal Properties (Karlheinz Schwarz, Techn. Universität Wien, Austria), 2001. ISBN 3-9501031-1-2.
9. K. Schwarz, J. Solid State Chem. 176, 319 (2003).
10. J. P. Perdew, K. Burke, and M. Ernzerhof, Phys. Rev. Lett. 77, 3865 (1996).
11. A. A. Mostofi, J. R. Yates, Y.-S. Lee, I. Souza, D. Vanderbilt, and N. Marzari, Comput. Phys. Commun. 178, 685 (2008).

12. J. Kuneš, R. Arita, P. Wissgott, A. Toschi, H. Ikeda, and K. Held, Comput. Phys. Commun. 181, 1888 (2010).

Figures

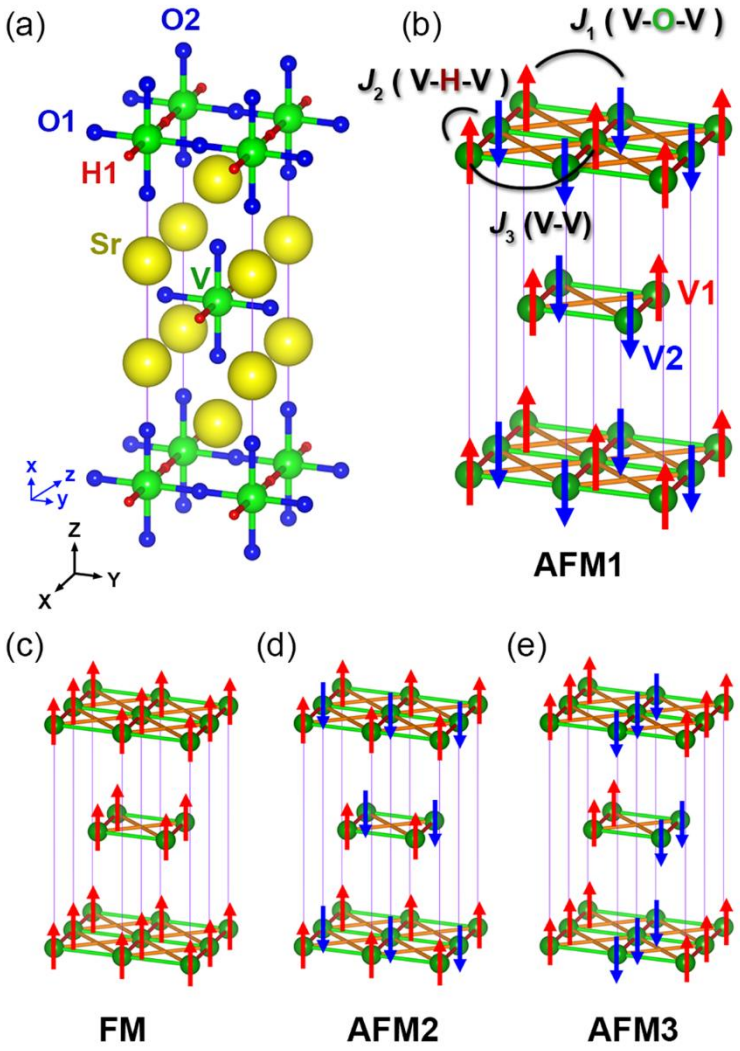

Figure 4-1. Crystal structure and ordered spin states of Sr_2VO_3H. (a) Crystal structure of the anion-ordered layered oxyhydride Sr_2VO_3H. Note that the H^- ions occupying O^{2-} sites are ordered linearly. The coordinate system for the DFT calculation is marked by blue arrows with *x*, *y*, and *z*. (b)–(e) Schematic representations of the four ordered spin states AFM1 (checker board), AFM2 (stripe), AFM3 (stripe), and FM of Sr_2VO_3H. J_1, J_2, and J_3 indicate the exchange coupling constants through the V–O–V, V–H–V, and V–V interaction pathways, respectively.

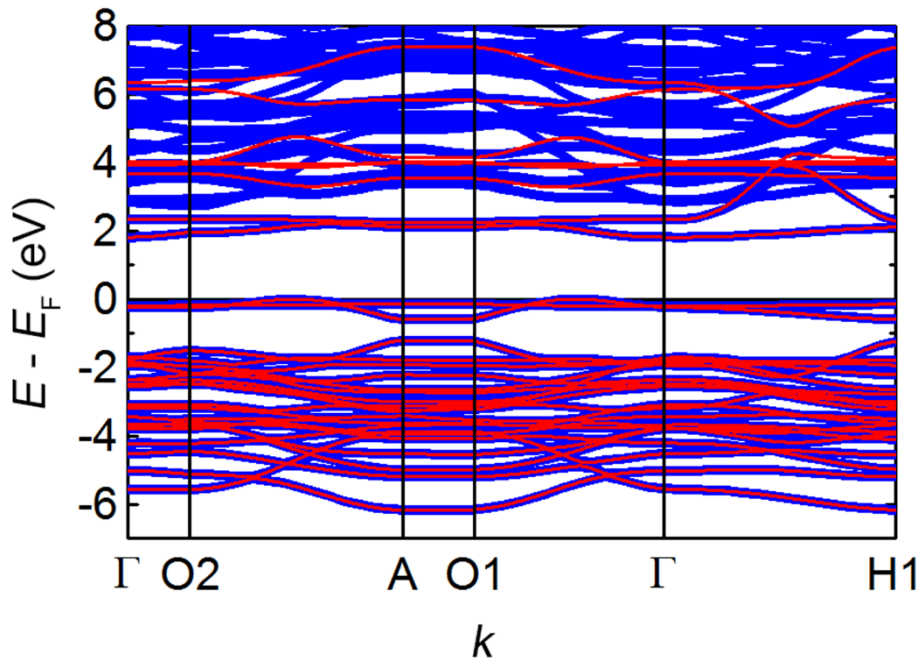

Figure 4-2. Electronic structure from the GGA+*U* calculation (blue curves) and the corresponding MLWFs (red curves) using 30 Wannier functions (**Table 4-1**). A frozen energy window of −7.0 to 2.5 eV was used to collect the Wannier functions.

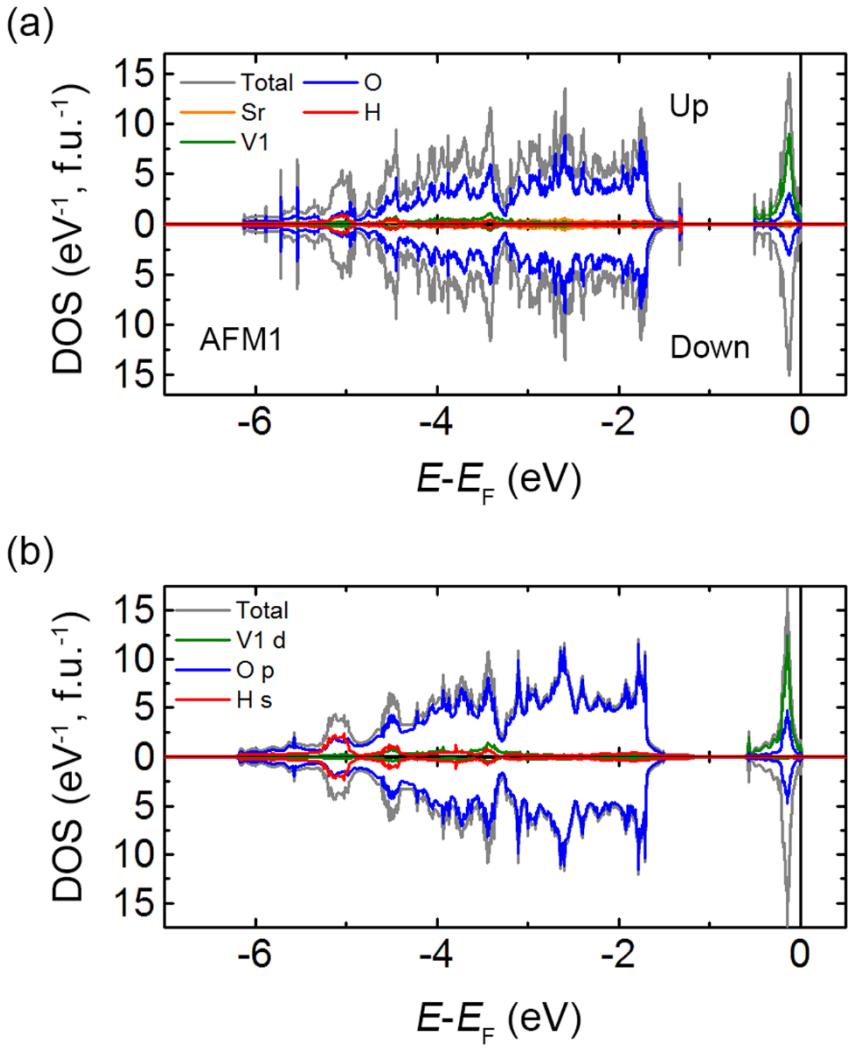

Figure 4-3. Comparison of the DOS from the (a) GGA+*U* and (b) MLWF calculations.

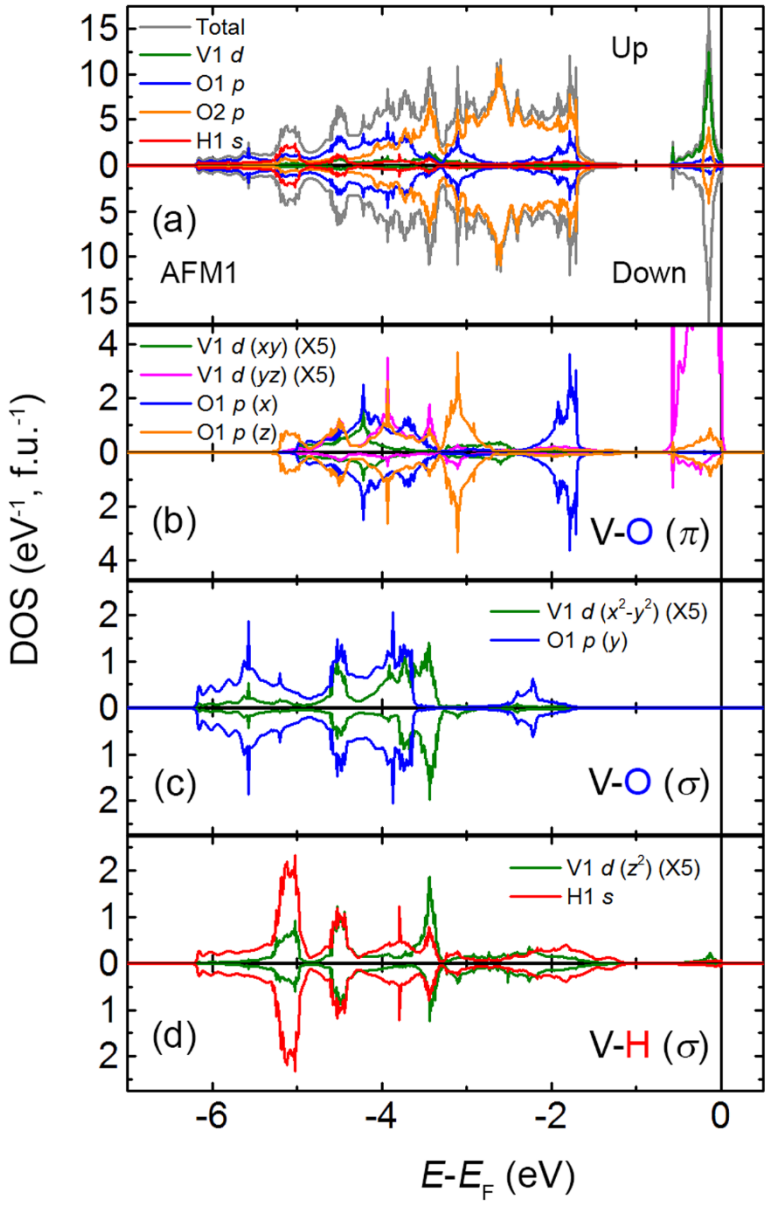

Figure 4-4. Total DOS and atomic PDOS for the AFM1 model using MLWFs based on the results of a GGA+*U* calculation with *U* = 3.5 eV. The total DOS is the sum of the PDOSs of V, O, and H (excluding Sr). The direction along the V–H bond is set to the *z* axis.

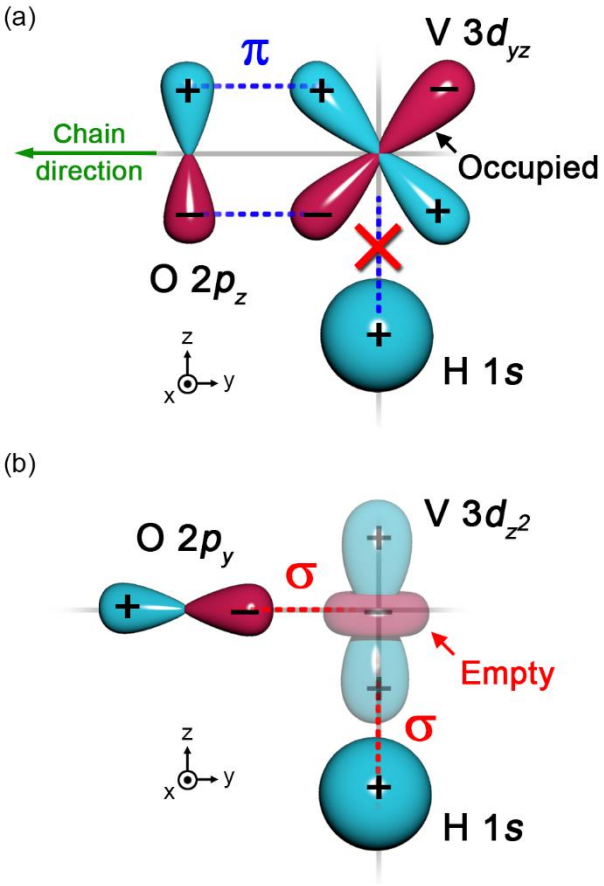

Figure 4-5. Schematic diagram of the orbital interaction to explain magnetic low-dimensionalization by hydride ion substitution. Hydride ion substitution breaks the π-exchange interaction between the *TM* and an oxide ion.

Table 4-1. Spreads (spin up/down) of the Wannier functions for the separate V *d*, O *p*, and H *s* bands.

Wannier function	Spread
V1 d_{xy}	1.6240/0.8697
V1 d_{xz}	0.9925/0.8632
V1 d_{yz}	0.9392/0.8989
V1 $d_{x^2-y^2}$	0.6311/0.6431
V1 d_{z^2}	1.1909/1.0851
V2 d_{xy}	0.8697/1.6240
V2 d_{xz}	0.8632/0.9925
V2 d_{yz}	0.8989/0.9392
V2 $d_{x^2-y^2}$	0.6431/0.6311
V2 d_{z^2}	1.0851/1.1909
O1 p_x	1.0980/1.0743
O1 p_y	1.2853/1.2279
O1 p_z	1.2465/1.2372
O2 p_x	1.0980/1.0743
O2 p_y	1.2853/1.2279
O2 p_z	1.2465/1.2372
O3 p_x	1.1365/1.1364
O3 p_y	0.8474/0.8474
O3 p_z	1.1199/1.1199
O4 p_x	1.1365/1.1364
O4 p_y	0.8474/0.8474
O4 p_z	1.1199/1.1199
O5 p_x	1.0743/1.0980
O5 p_y	1.2279/1.2853
O5 p_z	1.2372/1.2465
O6 p_x	1.0743/1.0980
O6 p_y	1.2279/1.2853
O6 p_z	1.2372/1.2465
H1 *s*	1.3014/1.3013
H2 *s*	1.3014/1.3013
Total	32.8861/32.8861

Table 4-2. Relative total energies ΔE (meV/unit cell) of the FM, AFM1, AFM2, and AFM3 spin models and exchange coupling constants J (meV) for various values of U (eV).

U	FM	AFM1	AFM2	AFM3	J_1	J_2	J_3	J_1/J_2
1.5	0	−299.46	−30.11	−252.93	−65.29	−9.58	1.03	6.82
2.5	0	−255.79	−34.84	−217.30	−54.78	−9.17	0.23	5.98
3.5	0	−216.85	−28.33	−184.50	−46.63	−7.59	0.25	6.15
4.5	0	−185.54	−23.23	−158.13	−40.05	−6.33	0.26	6.33

Table 4-3. Hopping integrals (eV) between V 3*d* and O 2*p*, and V 3*d* and H 1*s* orbitals in Sr_2VO_3H (spin up/down) and the number of unpaired spins for each V 3*d* orbital (Occ., %).

	O1 p_x	**O1 p_y**	**O1 p_z**	**O2 p_x**	**O2 p_y**	**O2 p_z**	**H1 s**	**Occ.**
V1 d_{xy}	1.15/1.18	0.00/0.00	0.00/0.00	0.00/0.00	1.02/1.02	0.00/0.00	0.00/0.00	2.1
V1 d_{xz}	0.00/0.00	0.00/0.00	0.00/0.00	0.00/0.00	0.00/0.00	1.04/1.21	0.00/0.00	48.1
V1 d_{yz}	0.00/0.00	0.00/0.00	1.17/1.34	0.00/0.00	0.00/0.00	0.00/0.00	0.00/0.00	45.4
V1 $d_{x^2-y^2}$	0.00/0.00	1.82/1.82	0.00/0.00	1.69/1.70	0.00/0.00	0.00/0.00	0.06/0.06	1.9
V1 d_{z^2}	0.00/0.00	0.69/0.78	0.00/0.00	0.58/0.67	0.00/0.00	0.00/0.00	2.20/2.15	2.5

Chapter 5 General Conclusions

Investigation of *TM* oxide compounds have been a fertile field for the discovery of new materials with intriguing physical properties. Considering the important role of the intervening anions, which mediate electronic and magnetic interaction between *TM* cations, investigation of mixed-anion compounds is a promising way to discover families of functional *TM* compounds. The hydride ion only forms σ bonds because hydrogen only has a 1*s* orbital, unlike other anions such as oxygen and the halogens. Such uniqueness can lead to completely different bonding interactions with *TM* cations.

In the present study, new layered perovskite oxyhydrides $Sr_2VO_{4-x}H_x$ were synthesized by high pressure solid state reaction and the effect of anion orbital symmetry on the chemical and physical properties of the *TM* compounds were investigated.

In Chapter 2, new layered perovskite vanadium oxyhydrides $Sr_2VO_{4-x}H_x$ ($0 < x < 1$) were synthesized and their crystal structures were characterized. By substituting H^- into the O^{2-} site, the hydrogen atoms selectively replace equatorial oxygen sites in V–O planes rather than apical oxygen sites, even before any structural transition occurs. A structural transition from a tetragonal (space group *I*4/*mmm*) to an orthorhombic (*Immm*) phase occurs because of a high degree of order of the hydride ions in the metal-oxide planes. The hydride ion ordering and the subsequent crystallographic transition can be explained by switching of the HOMO level from the ($d\pi$–$p\pi$)* antibonding molecular orbital to a lower energy $d\sigma$–$s\sigma$ bonding molecular orbital.

In Chapter 3, low-dimensionalization of magnetic ordering was found in a *TM* oxide

Sr_2VO_4 by substitution of O^{2-} with H^-. Upon increasing x in $Sr_2VO_{4-x}H_x$, the hydride ions ordered linearly and the magnetic susceptibility was simultaneously suppressed above the Néel temperature (160 K). The magnetic suppression was attributed to the formation of a 1D AFM spin-chain maintaining that each of the vanadium cations is two-dimensionally bridged by hydride and oxide ions.

In Chapter 4, theoretical calculations were performed to investigate the origin of the 1D magnetic behavior in a *TM* oxyhydrides $Sr_2VO_{4-x}H_x$. The results showed that the substitution of a hydride ion for an oxide ion breaks the π-exchange interaction between the *TM* ion and the oxide ion. This causes an anisotropic exchange interaction ($J_1/J_2 \sim 6$) originating from the absence of π bonding between H 1*s* and V 3*d* orbitals.

The results of this thesis suggest a different method to realize novel chemical and physical phenomena of *TM* compounds by utilizing heteromorphic mixed anions.

Acknowledgments

The present study was carried out under the supervision of Prof. ***Hideo Hosono***, Associate Prof. ***Hidenori Hiramatsu***, and Assistant Prof. ***Satoru Matsuishi*** (currently Associate Prof. at the Tokyo Institute of Technology) of the Tokyo Institute of Technology from April 2012 to September 2015.

First of all, from the bottom of my heart, I would like to thank Prof. ***Hideo Hosono*** for his precise guidance and continuous encouragement throughout the work. He has given me the chance to work in the research area of "Hydrogen in Oxides" and given much valuable advice during the entire period of my doctoral course. I would also like to express my sincere thanks to Prof. ***Toshio Kamiya*** and Associate Prof. ***Hidenori Hiramatsu*** for their guidance and valuable advice. I would like to thank Associate Prof. ***Satoru Matsuishi*** for his scientific guidance and practical advice. He has been a wise adviser and practical mentor for me throughout my research. I would like to thank Prof. ***Pung Keun Song*** for his scientific guidance and valuable advice. He has given me the opportunity to enter the research field of Materials Science and Engineering and provided guidance for fundamental research techniques.

I wish to thank Associate Prof. ***Tomofumi Susaki*** and Associate Prof. ***Toshiyuki Atou*** for their critical reading of this thesis and their useful comments.

I would also like to thank Prof. ***Hideya Kumomi***, Prof. ***Kenji M. Kojima***, Prof. ***Osamu Fukunaga***, Prof. ***Satoru Fujitsu***, Prof. ***Toshiya Otomo,*** Associate Prof. ***Haruhiro Hiraka***, Associate Prof. ***Hechang Lei***, Associate Prof. ***Hiroshi Mizoguchi***, Associate Prof. ***Jun-ichi Yamaura***, Associate Prof. ***Sung Wng Kim***, Associate Prof. ***Tomofumi Tada***, Assistant Prof.

Fuji Funabiki, Assistant Prof. ***Kimoon Lee***, Assistant Prof. ***Soshi Iimura***, Assistant Prof. ***Yoshitake Toda***, Dr. ***Dong Hee Lee***, Dr. ***Fumitaka Hayashi***, Dr. ***Gihun Ryu***, Dr. ***Jiangang Guo***, Dr. ***Kyeongmi Lee***, Dr. ***Sehoon Jeong***, Dr. ***Taku Hanna***, Dr. ***Yanpeng Qi***, Dr. ***Yoshinori Muraba***, Mr. ***Hikaru Sato***, Mr. ***Junghwan Kim***, Mr. ***Jun-ichi Ishida***, Mr. ***Sang-Won Park***, Mr. ***Shizuo Hayashi***, Mr. ***Yudai Tomota***, Mr. ***Yuji Kondo***, and Ms. ***Yukiko Obata*** for their kind guidance, discussions, and important suggestions.

I also would like to acknowledge Secretaries Ms. ***Hanae Murayama***, Ms. ***Kanako Ochiai***, and Ms. ***Mayumi Nakano***.

Finally, I express appreciation to my family and friends.

September 2015

Joonho Bang

Publications

Papers included in the thesis

1. "Hydrogen Ordering and New Polymorph of Layered Perovskite Oxyhydrides: $Sr_2VO_{4-x}H_x$"

   Joonho Bang, Satoru Matsuishi, Haruhiro Hiraka, Fumika Fujisaki, Toshiya Otomo, Sachiko Maki, Jun-ichi Yamaura, Reiji Kumai, Youichi Murakami, and Hideo Hosono

   Journal of the American Chemical Society, **136**, 7221 (2014).

2. "Low dimensionalization of Magnetic Ordering in Sr_2VO_4 by Hydride Ion Substitution"

   Joonho Bang, Satoru Matsuishi, Sachiko Maki, Jun-ichi Yamaura, Masatoshi Hiraishi, Soshi Takeshita, Ichihiro Yamauchi, Kenji M. Kojima, and Hideo Hosono

   Physical Review B, **92**, 064414 (2015).

Other papers

3. "Crystal Structure and Physical Properties of New Transition Metal Based Pnictide Compounds: La*TM*$_2$AsN (*TM* = Fe, Co, and Ni)"

   Sehoon Jeong, Satoru Matsuishi, Joonho Bang, and Hideo Hosono

   APL Materials, **3**, 041509 (2015).

Presentations

1. “Hydrogen in Layered Perovskite Oxides: Synthesis and Crystal Structure of $Sr_2VO_{4-x}H_x$”. The Ceramic Society of Japan: Annual Meeting, March 19 (2014).

2. “Hydrogen Ordering Induced Structural Transition in $Sr_2VO_{4-x}H_x$”. The Eighth International Conference on the Science and Technology for Advanced Ceramics, June 27 (2014).